Sulphur solubility and sulphide immiscibility in silicate melts as a function of the concentration of manganese, nickel, tungsten and copper at 1 atmosphere and 1400 °C

K.A. Evans [a,*,1], H. St.C. O'Neill [a] J.A. Mavrogenes [a]

[a] *Research School of Earth Sciences, Building 61, Mills Road, Australian National University, Acton 0200, Australia*

Abstract

Solubility and immiscibility relationships in silicate melts as a function of the concentrations of Cu, Mn, Ni and W were measured for melts synthesised at 1400 °C and 1 bar. Relationships between fS_2, fO_2 and the S solubility were also investigated. The results were used to extend and calibrate an existing model for the solubility of S in silicate melts to Mn- and W-bearing melt compositions. Mn was found to enhance S solubility. W was found to have little effect on S concentration. Ni stabilised an immiscible sulphide phases at metal contents higher than 0.01 to 0.05 wt %. Cu was lost from the samples, this was attributed to the formation of an immiscible sulphide phase or devolatilisation of Cu as a Cu-S vapour phase.

The data was consistent with an expression for S solubility of the form $\ln[S] = A_0 + \sum_M X_M A_M + 1/2 \ln \frac{fS_2}{fO_2}$, where X_M is the mole fraction of cation M and the A terms are calibration constants. A_M values for Mn and W are 29.5 ± 1.7 and 8.54 ± 6.91 respectively. The expression was tested against other models, and on

experimental data that was not included in the calibration. Observed and calculated values were in good agreement. The data for Cu and Ni are consistent with extant thermodynamic models for sulphide saturated silicate melts. These metals effectively stabilise sulphide melt phases, with implications for our understanding of the formation of magmatic sulphide ore deposits and the fractionation of chalcophile elements.

Key words: sulphur, silicate melt, copper, nickel, tungsten, manganese, experiment

1 Introduction

A quantitative understanding of the solubility of sulphur in silicate melts is necessary if we are to understand a wide range of processes that include global sulphur cycling (e.g. Alt et al., 1993; Fischer et al., 1998), the formation of economic sulphide deposits (e.g Cawthorn, 2005; Lee and Ripley, 1995; Li and Ripley, 2005; Pina et al., 2006), the distribution of chalcophile elements such as platinum, rhenium, osmium and palladium (e.g. Naldrett, 1999; Wang and Zhou, 2006), and the effects of volcanic eruptions on the atmosphere (e.g. de Hoog et al., 2004).

Much work on the solubility of sulphur in silicate melts has been performed by metallurgists (e.g. Fincham and Richardson, 1954; Seo and Kim, 1999; Shankar et al., 2006; Young et al., 1992). However, such work is of limited use to earth scientists because the compositions and conditions of formations of these

* Corresponding author.
Email address: k.evans@curtin.edu.au (K.A. Evans).
[1] Now at: School of Applied Geology, Curtin University, GPO Box 1987, WA6845, Australia.
tel: 0061 8 92664682
fax: 0061 8 92663153

slags are far from those of geological interest. Other work (e.g. Buchanan and Nolan, 1979; Buchanan et al., 1983; Haughton et al., 1974; Jugo et al., 2005; Katsura and Nagashima, 1974; Liu et al., 2007; Mavrogenes and O'Neill, 1999; O'Neill and Mavrogenes, 2002; Shima and Naldrett, 1975) has investigated the solubility of sulphur in silicate melts that range from basaltic to rhyolitic compositions, at pressures to 1 GPa, temperatures to 1400°C, and with and without the presence of water and/or a coexisting immiscible sulphide phase.

Experimental data has been combined with data from natural samples to produce expressions that predict sulphur solubility as a function of melt composition and extensive parameters such as pressure, temperature, fO_2 and fS_2 (e.g. Fincham and Richardson, 1954; O'Neill and Mavrogenes, 2002; Moretti and Ottonello, 2005; Scaillet and Pichavant, 2005; Wallace and Carmichael, 1992). Early work (e.g. Fincham and Richardson, 1954) was based on the assumption that sulphur substitutes for oxygen in silicate melts via

$$O^{2-}_{\text{melt}} + 1/2S_{2,\text{gas}} = S^{2-}_{\text{melt}} + 1/2O_{2,\text{gas}} \quad (1)$$

at oxygen fugacities sufficiently reducing that S^{2-} is the dominant sulphur species in the melt. The equilibrium constant for this reaction can be arranged to produce the Fincham-Richardson relationship (Fincham and Richardson, 1954; Eqn 2)

$$\ln C_S = \ln [S] + 1/2 \ln fO_2/fS_2 \quad (2)$$

where C_S is the sulphide capacity in wt%, which is a function of pressure, temperature, and melt composition, and [S] is the sulphur concentration, also in wt%. Deviations from the model were noted by some studies (e.g. Buchanan

and Nolan, 1979; Buchanan et al., 1983). The experimental data from these studies was used as the basis for more complex formulations (e.g. Poulson and Ohmoto, 1990). However, extensive testing of the Fincham-Richardson relationship by O'Neill and Mavrogenes (2002) showed that most of these deviations could be attributed to experimental error. It is therefore reasonable to prefer theoretical models that are consistent with the Fincham-Richardson relationship. One such model, that combines a relatively small number of calibration parameters with a robust thermodyamic background, is that of O'Neill and Mavrogenes (2002). This model combines the conceptual model that underlies the Fincham-Richardson relationship with an fused salt thermodynamic model for silicate melts to produce an expression (Eqn 3) for the sulphide capacity at 1400°C and 1 bar as a function of melt composition (O'Neill and Mavrogenes, 2002).

$$\ln C_{\mathrm{S}} = A_0 + \sum_M X_M A_M \tag{3}$$

where C_{S} is the sulphide capacity and X_M is the mole fraction of cation M. A_0 is a constant that combines the conversion factor between the mole fractions and wt% concentration scale with the activity coefficient for the sulphur species in the melt. The A_M are coefficients that represent the tendency of a metal to prefer a sulphur neighbour in a melt over an oxygen neighbour via the difference in chemical potentials of the oxide and sulphide melt component. Full details and derivation of this expression are provided by O'Neill and Mavrogenes (2002). This expression successfully describes the solubility of S in silicate melts in the system CaO-FeO-TiO_2-MgO-Al_2O_3-SiO_2-S over a wide range of compositions.

However, there are a number of elements other than CaO-FeO-TiO_2-MgO-

Al_2O_3-SiO_2-S that are present in silicate melts and that might be expected to have a significant effect on the sulphide capacity of a melt. The principal among these are metal cations that form sulphide phases, such as copper, manganese and nickel. Iron, which is a sulphide-forming cation, has a large effect on the sulphide capacity of melts, indeed, the sulphide capacity of melts with a Fe content around 10 wt% (typical of terrestrial basalts) is controlled mostly by the Fe content (O'Neill and Mavrogenes, 2002). The other transition metals (e.g. Cu, Mn, Ni) might be expected to have similar properties, as might W, which forms stable sulphides under a wide range of conditions. There is some evidence that Ni enhances S solubility in a similar way to iron; Li et al. (2003) have argued that the Ni partition coefficient between melt and olivine is correlated with the S content of natural basaltic melts, which indicates that the two elements have some affinity. Apart from this, there is little evidence, experimental or natural, of the effect that metals such as Mn, Cu, Ni and W can have on the S content of silicate melts. An understanding of these effects is critical if metal-sulphur systematics in potentially ore-forming deposits are to be understood.

An additional aspect of interest is the equilibration of a S-bearing silicate melts with an immiscible sulphide melt. Such sulphide melts play an important role in the formation of magmatic ore deposits (e.g. Mungall, 2002), metamorphosed sulphide-bearing ore deposits (e.g. Mavrogenes et al., 2001), and the fractionation of chalcophile elements such as rhenium and osmium. The presence of a sulphide melt phases imposes a maximum on the S content of a silicate melt and this additional constraint can be incorporated into the thermodynamic description of the S content of silicate melts (e.g. O'Neill and Mavrogenes, 2002).

The purpose of this study is to measure the effects of Cu, Mn, Ni and W on the solubility and immiscibility of S in silicate melts at 1400°C and 1 bar. The results are used to calibrate the model of O'Neill and Mavrogenes (2002) for these metals to produce a more general model for the prediction of the sulphide capacity of silicate melts.

2 Methods

Oxides and carbonates were mixed in the appropriate proportions to provide the starting materials for the silicate glasses. The runs used in the thermodynamic analysis utilised an anorthite-diopside eutectic mix with added Ca (ADeu + Ca). The Ca was added to increase the base level S concentration in the samples, which reduces analytical uncertainties. A number of samples were prepared with zero additive metal content to establish the baseline S content for the study. These samples were included in several of the runs listed in Table 1. Analysis of these samples allows the repeatability of runs at identical theoretical fO_2 and fS_2 values to be assessed. In most other runs, oxides were added to the mixes in concentrations that varied from 0.1 wt % to 10 wt%. Sample notation is of the form B*xxxxxx*p*y*, where *xxxxxx* indicates the date of the run, and *y* indicates the sample number from that run. The intended additive metal concentrations for runs labelled B*xxxxxx* low in Table 1 were 0, 0.2, 0.4, 0.6, 0.8 and 1.0 wt%, and for runs labelled B*xxxxxx* high were 0, 2, 4, 6, 8 and 10 wt%. The exceptions were run B070406, which contained Ni at 10, 15, 20, 25 and 30 wt %, and B270306 which contained Mn at 3.5 wt% in all the samples except a zero Mn-sample. Not all the samples were retrieved from all the runs.

The oxides and carbonates were mixed under acetone and were mixed with polyethylene oxide to form a thin paste. The paste was mounted onto 3-5 mm diameter rhenium wire loops which were loaded into the vertical muffle tube furnaces where they were converted to silicate glasses. The furnaces used for this study are modified to allow accurately measured gas mixes to flow upwards through the furnace. fO_2 and fS_2 were controlled by the proportions of CO, CO_2 and SO_2, which were supplied to the furnace by Tylan F2800 mass flow controllers. Values of fO_2 and fS_2 corresponding to the input gas mixes were calculated as described by O'Neill and Mavrogenes (2002). Uncertainties in fO_2 and fS_2 are estimated to be $\pm$ 0.05 log units (c.f. O'Neill and Mavrogenes, 2002). Gas flow rates and calculated fugacities for O_2, S_2 and SO_2 are given in Table 2.

It was possible to run six samples at a time, and these were loaded while the furnace was at a temperature of around 600°C. This low temperature was used to prevent the samples sticking to each other if they accidentally touched during loading. When loading was complete the CO and CO_2 gases were switched on and the temperature was increased at 6 °C per minute up to 1400 °C. The SO_2 flow was switched on once temperatures rose above 1000°C. Samples were run for 24 hours. Previous work (O'Neill and Mavrogenes, 2002) has suggested that this time is sufficient for equilibration between the glass and the input gases even when immiscible sulphide melts are formed. After 24 hours the runs were quenched by releasing the wire loops into water. A small number of experiments were quenched in air to test the effect of the different quenching mechanisms. Most of the experiments were performed at an fO_2 of -9.6 and a log fS_2 of -1.91. These conditions have the advantage that they produce high S contents ($>$ 0.2 wt % in most cases) without any

risk of blocking the furnace with precipitated elemental S, which can be the case when SO_2 flow rates are high. Cu experiments were undertaken at slightly more oxidising conditions with a log fO_2 of -8.1 and a log fS_2 of -1.91. These conditions were chosen in an attempt to decrease Cu loss, a phenomenon that had been noted during trial experiments (unpublished results). Experiments on Mn-, W- and Ni-bearing melts were also undertaken at more oxidising conditions, with log fO_2 set to -7.6, -7.18 and -3.1. fS_2 in these experiments was kept as high as possible without running the risk of blocking the furnace with precipitated elemental sulphur. The purpose of these experiments was to test the Fincham-Richardson relationship for Cu, Ni, W and Mn. Subsequent text will, for the sake of convenience, refer to experiments performed at a log fO_2 of -9.6 and a log fS_2 of -1.91 as group 1 experiments, to those performed at a log fO_2 of -7.18 and a log fS_2 of -1.81 as group 2 experiments, to those performed at a log fO_2 of -7.6 and a log fS_2 of -2.8 of as group 3 experiments, and to those performed at a logfO_2 of -3.09 and a log fS_2 of -11.88 as group 4 experiments. 31 successful runs were completed, with 4-6 samples produced for each. Several of the runs were duplicated, to assess the repeatability of the experiments and to provide samples for synchrotron analysis.

The glass samples were set in epoxy and polished before analysis. The samples were then examined optically for evidence of exsolution of immiscible sulphide liquids and the formation of silicate crystal phases. The existence of phases other than silicate melt does not invalidate the use of samples in this study, so long as equilibrium is attained, but the presence of additional phases reduces the variance of the assemblage and interpretations need to be carried out accordingly. The samples were then carbon-coated and analysed for major elements and the trace metals Cu, Mn, W and Ni on the Cameca SX100

electron microprobe at the Research School of Earth Sciences at the Australian National University. WDS analysis and a 15 KeV accelerating voltage was used for all elements. Raw counts were converted to element weight percentages using a modified ZAF correction scheme. The major elements were analysed first using a 10 nA, 15 KeV beam with a 10 micron radius. Sulphur and the trace metals were subsequently analysed using a 100 nA, 20 micron beam.

Sulphur was analysed using a peak area routine to eliminate artefacts arising from the dependence of the peak position on sulphur oxidation state. Two of the WDS spectrometers attached to the machine were scanned across the sulphur peak, and the total counts were integrated to obtain the sulphur measurement. Scan time was 150 seconds, and the peak measurement occurred between channels 61293 to 61493 on the LPET crystal. 48 channels on either side of the peak were scanned to obtain a background measurement. The calibration standard for S analysis was a mixture of FeS and $CaSO_4.2H_2O$ for the early runs (to B110406) and $CaSO_4.2H_2O$ for subsequent runs. The secondary standards were NIST610 and VG2 (Jarosewich et al., 1979) and these were run at least every four hours over the course of the analysis. The average value for NIST610 over the course of the analysis presented here was 0.056 $\pm$ 0.006 wt %, which compares well with the 0.058 wt % for this standard that is reported by O'Neill and Mavrogenes (2002). The average S concentration in VG2 was 0.143 $\pm$ 0.05 wt %, which also agrees well with reported values. Previous determinations include 0.14 $\pm$ 0.003 wt % (O'Neil and Mavrogenes, 2002); 0.134 $\pm$ 0.008 wt % (Dixon et al., 1991); 0.142 $\pm$ 0.004 wt % (Wallace and Carmichael, 1992); 0.14 wt % (Nilsson and Peach, 1993); 0.137 $\pm$ 0.003 wt % (Thordarson et al., 1996); 0.145 $\pm$ 0.003 wt % (Metrich et al., 1999); and 0.142 $\pm$ 0.004 wt % (de Hoog et al., 2001). Values for Mn, Cu and Ni obtained

from NIST610 were 0.048 ± 0.003 wt %, 0.049 ± 0.003 wt % and 0.053 ± 0.004 wt % respectively, which also agree well with reported values (Pearce et al., 1997) of 0.042 ± 0.008 wt % for Mn, 0.042 ± 0.002 wt % for Cu, and 0.044 ± 0.008 wt% for Ni. All uncertainties are one standard deviation. Four or five points were analysed on each piece of glass. Care was taken to measure points evenly distributed across the whole piece of the glass, and the similarity of the points was used as a test for equilibrium. If the standard deviation of the additive metal or sulphur from the multiple analyses was greater than 5%, or 0.015 wt%, whichever was the larger, then disequilibrium was suspected and the results treated with caution. Analyses for such samples are marked with an asterisk in Table 3. Samples with additive metal and S contents below the detection limits of 0.015 wt%, for S and W, 0.01 wt %, for Cu and Mn, and 0.005 wt %, for Ni, were rejected. Detection limits were given by the Cameca software, based on the counting statistics.

Parameters that contribute significantly to uncertainties in C_S are values of fO_2 and fS_2 for the input gas mixes and the measured S concentration. Uncertainties in fO_2 and fS_2 are estimated to be ± 0.05 log units (c.f. O'Neill and Mavrogenes, 2002). Uncertainties for S concentration based on counting statistics are provided by the Cameca software; uncertainties on the S content were less than ± 0.015 wt % in all cases. These uncertainties were propagated through the equation for C_S (Eqn 2) to obtain the error bars shown (Figs 1 to 5). Uncertainties in additive metal contents are estimated to be ± 0.01 wt % for Mn, Ni and Cu, and ± 0.015 wt % for W.

Selected samples with Ni and Cu concentrations below probe detection limits were analysed on the LA-ICPMS (Laser Ablation-Inductively Coupled Plasma Mass Spectrometer) at the ANU. Ablation was performed in a He atmosphere

by an ArF EXIMER laser (193 nm) with a pulse energy of 120 mJ and a 5 Hz pulse repetition rate; the ablation time was 40 s, with 20 s spent measuring background prior to the ablation. A laser spot size of 142 m was used. The ablated material was flushed in a continuous argon flow into the torch of an Agilent 7500 Series ICP-MS. The silicate glass reference material NIST 610 (National Institute of Standards and Technology) was used as the external standard with 29Si as the internal standard. Further information regarding correction procedures, limits of detection and instrumental errors can be found in Eggins et al. (1998).

3 Results

3.1 Sample appearance and approach to equilibrium

Most of the samples formed translucent clear or yellow-coloured glass beads. Some remained in one piece during the quenching process and some fractured. Unfractured samples were up to 5mm diameter and weighed between 0.05 and 0.15g. Many samples (Table 3) contained bubbles and/or black specks. In most cases the black specks occurred on the margins of the sample, or showed dendritic form in fractures. In Ni-bearing samples the specks were distributed through the glass and appeared to define flow patterns. Generally the black specks were <5 microns in size and could not be analysed. However, in two Ni-bearing samples, B220306p6, and B070406p6, there was sufficient black material exposed for analysis (Table 3c). The material was found to consist of nickel and sulphur with a small amount of iron; atomic Fe/(Fe+Ni)< 0.06. Black specks in the other samples are therefore inferred to be sulphides

produced on surfaces or fractures during quench. Microprobe analyses did not sample these areas as fractures and rims were avoided, and good compositional repeatability was obtained in over 90% of the samples analysed (Table 3). This suggests that equilibrium was attained in most cases. Attainment of equilibrium did not depend systematically on the identity of the additive metal or run conditions; the percentage that apparently reached equilibrium for Cu, Mn, Ni and W was 100, 92, 89 and 87 % respectively. However, Ni-bearing samples that show a larger variation between analyses do differ noticeably from the others in terms of their sulphide capacity - Ni content systematics; this is discussed in more detail below.

A number of samples (Table 3) had a lower Ca content than that intended, with drops in Ca content of up to 10 wt%. Drops in Ca content occurred in Mn-, Ni-, and W-bearing samples, and the feature was more common, for Mn and W, in those samples with high additive metal content (Mn $>$ 8 wt%, W $>$ 2 wt%) from runs with low fO_2. Samples with low Ca contents did not preferentially exhibit disequilbrium compared to the higher Ca samples. The number expected to show disequilibrium and low Ca, based on a simple proportional calculation, which would be appropriate if the two features were unrelated was 0, 1 and 3, for Mn, Ni and W respectively, whereas the observed numbers were 0, 2 and 3. This suggests that the process that caused the low Ca contents did not induce disequilibrium. Attempts were made to locate and analyse the Ca-bearing phase on the microprobe. However, such a phase could not be found or analysed. This detracts from the completeness of the study, however, interpretation and conclusions of the study with respect to sulphur solubility systematics are unaffected.

3.2 Sulphur concentrations

The runs without additive Mn, W, Ni or Cu produced a baseline S content for the ADeu + Ca composition of 0.199 ± 0.026 wt % (n=19). Some of the variation observed can be attributed to small quantities of Fe in the samples, which was detected by the electron microprobe. No Fe was added to the mixes, therefore Fe in the samples is likely to have come from contamination in the furnaces. The compositions of air-quenched runs were indistinguishable from those of the water-quenched runs but results from these samples are not included here.

Sulphur content was positively correlated with Mn concentration for the data from the Mn-bearing group 1, 2 and 3 experiments (Table 3a, Fig 1a). Melts produced under more oxidising conditions (groups 2 and 3) showed a less extreme dependence of S solubility on Mn content than the most reducing (group 1) melts, where S concentrations of up to 1 wt% were measured in the most Mn-rich (Mn close to 10 wt%) glasses. Sulphur in the group 4 samples (B180906), which had the most oxidising conditions of formation, is below detection limits. The experiments show good repeatability. For example if B030106 is compared with B151106, sulphur concentrations for equivalent samples are repeatable within 2% and Mn concentrations within 5 wt%.

Results for the W-bearing glasses depend on the initial W content of the melt (Table 3b, Fig 1b). Glasses produced by runs with initial W contents of less than 1 wt % (B150906 and B301205) have a S content of around 0.2 wt %, a Ca content of around 24 wt %, and show no systematic relationship between W content and S. Glasses produced by runs with an initial W content higher than

1 wt% (B240306 and B220806) exhibit a reduced Ca, at 14 - 16 wt% which suggests the exsolution of a Ca-bearing phase. This phase was not exposed at the surface of the glass and so could not be investigated with the microprobe. The W content of the samples unaffected by the Ca loss, but the S content of these high W glasses is much lower than for the low W glasses. S content is effectively independent of W content, as for the low W samples. In runs where log fO_2 was increased above -9.6 (groups 2, 3, and 4), the S content drops below detection limits for all samples with appreciable W. If W content is also high in these runs then the Ca content drops, as for the lower fO_2 runs (Table 3b: B230806 and B200906).

Some of the Ni-bearing glasses contain Ni or S in concentrations below the detection limits (Table 3c). The remainder of the samples lie on a trend that defines a reciprocal or pseudo-reciprocal relationship between S and Ni (Fig 1c). This is consistent with equilibration of the melt with a Ni sulphide phase, which was observed to have exsolved from the melt in many of the samples. All three groups of samples lie on the same reciprocal trend. The reciprocal relationship is strikingly different to the positive correlation between metal and S content that was found for Mn; compare Figs 1a and Fig 1c. Group 4 samples (B190906), which had the most oxidising conditions of formation, have high Ni contents, up to several wt%, but the S concentration in these samples is below the detection limit (B190906).

Cu and S contents in the Cu-bearing runs (Table 3d, Fig 1d) are close to, or below, the detection limits for one or both elements in all experiments. Cu was added to the samples in concentrations of up to 10 wt%, which is many times that found by analysis, so these results represent massive Cu loss. Black blebs of an exsolved phase inferred to be copper sulphide melt was observed

in some samples (Table 3d). Sulphur concentrations are much less than the baseline concentration for Cu-free samples (0.04 wt % vs. 0.199 wt %).

3.3 Sulphide capacities

Sulphide capacities calculated from Eqn 2 were plotted (Fig. 2). The Cu-bearing melts were omitted from this exercise because the low Cu and S concentrations prevent meaningful analysis of this parameter. The Mn-bearing melts (Fig. 2a) coalesce to form an approximately linear trend. This result is consistent with the Fincham-Richardson relationship.

In the W-bearing melts, (Fig. 2b,c), melts with high and low W content plot in different places in W - C_S parameter space. The high W samples (Fig. 2b) form a linear trend in C_S-W space with an approximately constant C_S. The low W samples form a similar trend, but at a lower C_S value.

The Ni-bearing melts (Fig. 2b) exhibit different characteristics for the Mn-bearing melts. Data taken from each set of fO_2/fS_2 conditions plot in different parts of the C_S parameter space, with the higher fO_2 experiments having both higher metal content and sulphide capacity. The data apparently records negative correlations between Ni and C_S for each group, although the analytical uncertainties are sufficiently large that the negative correlations are not statistically significant.

4 Discussion

4.1 Qualitative interpretation of concentration and sulphide capacity data

4.1.1 Manganese

Data from the Mn-bearing melts (Fig. 1a) are as expected for a system that obeys the Fincham-Richardson relationship and with S solubility specified by Eqn 3. Mn and S are positively correlated, with different slopes in S-Mn space for the different gas compositions. The data then coalesces into a single trend when sulphide capacity (Eqn 2) is plotted against metal content. A further test for the Fincham-Richardson relationship is to plot $\frac{1}{2}\log f_{S_2} - \log[\mathrm{S, wt\%}]$ against $\frac{1}{2}\log f_{O_2}$ (Fig. 3a). If the Fincham-Richardson relationship holds then the slope of the data should be 1. The data is consistent with, but does not uniquely define, such a line (Fig. 3a). The Mn data therefore suggests that sulphur dissolves in melts according to Eqn 1. The positive correlation between sulphide capacity and Mn further suggests that the presence of Mn induces a free energy incentive for dissolution of S via the formation of Mn-S ion pairs or some more complex melt species.

4.1.2 Tungsten

The difference between the sulphide capacity of the Ca-rich and Ca-poor W-bearing melts can be attributed to a change in melt composition driven by precipitation of a Ca-bearing phase. There is no evidence that the precipitation of such a phase has caused disequilibrium in the samples, so the existence of this phase does not affect the interpretation or conclusions given here. The

baseline sulphide capacity for the Ca-rich melts, calculated with Eqn 3 and the coefficients of O'Neill and Mavrogenes (2002) is 1.8 x 10^{-5} wt%. This is similar to the observed average for Ca-rich melts with W less than 1 wt %, which is 2 x 10^{-5} wt%. The calculated baseline sulphide capacity for the Ca-poor melts is 8 x 10^{-6} wt%. This compares well with the observed average for the sulphide capacity for the low W Ca-poor melts, which is 1.1 x 10^{-5} wt%. Once this difference in melt composition is accounted for, the characteristics of the W-bearing samples are consistent with a melt in which there is little free energy incentive for W-S nearest neighbours and thus little correlation between W and S contents of melts.

4.1.3 Nickel

Interpretation of the data from the Ni-bearing melts is complicated by the existence of a coexisting Ni sulphide phase which affects the Ni-S systematics. However, it is possible to predict Ni-S relationships for this situation (Fig. 3b,c). The location of the Ni-sulphide saturation surface is calculated based on the assumption that the coexistence of the silicate melt with a Ni sulphide phase can be represented by Eqn 4.

$$\mathrm{NiO_{melt}} + 1/2\mathrm{S_{2,gas}} = \mathrm{NiS_{sulphide\ melt}} + 1/2\mathrm{O_{2,gas}}. \quad (4)$$

The expression for K_4, which is the equilibrium constant of the equilibrium defined by Eqn 4, can be combined with Eqn 2 to give

$$[\mathrm{S}] = \frac{C_\mathrm{S}\{\mathrm{NiS_{sulphide\ melt}}\}}{K_4\{\mathrm{NiO_{melt}}\}} \quad (5)$$

Square brackets indicate concentration and curly brackets indicate activity, as is conventional. C_{S} and [S] are in wt %, while the activities of $\mathrm{NiS}_{\mathrm{sulphidemelt}}$ and $\mathrm{NiO}_{\mathrm{melt}}$ are relative to the chosen standard states for the sulphide and silicate melts. If the melt is assumed to consist of interlocking cation and anion lattices (Temkin model), where the standard state for any ion is 100% occupancy of the relevant lattice by that ion, and if the activity coefficients of Ni^{2+} and O^{2-} in the melt are $\gamma_{\mathrm{Ni}^{2+}}$ and $\gamma_{\mathrm{O}^{2-}}$ respectively, then

$$\{\mathrm{NiO}_{\mathrm{melt}}\} = \mathrm{X}_{\mathrm{Ni}^{2+}_{\mathrm{cation}}} \mathrm{X}_{\mathrm{O}^{2-}_{\mathrm{anion}}} \gamma_{\mathrm{Ni}} \gamma_{\mathrm{O}^{2-}}, \tag{6}$$

where X_i refers to the mole fraction of i on the cation or anion lattice. Eqn 5 can then be written as

$$[\mathrm{S}] = \frac{C_{\mathrm{S}}\{\mathrm{NiS}_{\mathrm{sulphide\ melt}}\}}{K_4 \mathrm{X}_{\mathrm{Ni}^{2+}_{\mathrm{cation}}} \mathrm{X}_{\mathrm{O}^{2-}_{\mathrm{anion}}} \gamma_{\mathrm{Ni}^{2+}} \gamma_{\mathrm{O}^{2-}}}. \tag{7}$$

Eqn 7 is equivalent to Eqn 24 of O'Neill and Mavrogenes (2002) if it is assumed that $\mathrm{X}_{\mathrm{O}^{2-}_{\mathrm{anion}}}$ is equal to 1, and if $\gamma_{\mathrm{Ni}}\gamma_{\mathrm{O}^{2-}}$ is equal to γ_{NiO}.

Eqn 7 predicts that the presence of a Ni sulphide phase imposes an approximately reciprocal relationship between Ni and S in the silicate melt phase which is insensitive to $f\mathrm{O}_2$ and $f\mathrm{S}_2$. The term on the right hand side would, however, be sensitive to melt composition, via the C_{S}, activity coefficient, and $[\mathrm{O}^{2-}]$ terms, but the variation in these parameters for the range of melts considered here is negligible and so the right hand side of Eqn 7 would be approximately constant for the melt compositions considered here. The value of K_4 can be estimated from thermodynamic data for Eqn 4; Gibbs energies for the relevant phases were taken from O'Neill and Eggins (2002) and Barin (1989). These data give a value for K_4 of 0.031 at 1400°C. The value of γ_{NiO}

is taken from O'Neill and Eggins (2002) to be 2.5. The position of the sulphur content at sulphide saturation (SCSS) line can then be calculated, assuming that $\{NiS_{\text{sulphide melt}}\}$ is equal to 1, and if A_{Ni} coefficient in Eqn 3 is specified. Calculated SCSS lines are shown in Figs 3a and b for A_{Ni} values of 30 and 254 respectively. The A_{Ni} value of 30 was chosen because it is similar to that for iron, which has an A_{Fe} of 26.3 (O'Neill and Mavrogenes, 2002), and the higher value was chosen to allow the effect of uncertainty in A_{Ni} values to be investigated. The line is given an arbitrary uncertainty of plus or minus a natural log unit. This is considered reasonable, given uncertainties of parameters such as the activity of NiS in the sulphide melt phase, the value of K_4, and the value of the activity coefficient, γ_{NiO}. A one log unit uncertainty in the position of the NiS-saturated line would be caused by a factor of e uncertainty in one of the activity coefficients or the activity of NiS in the sulphide melt, by an uncertainty in the value of the Gibbs energy of reaction 4 of 14 kJ mole^{-1}, or some combination of the above.

Ni and S contents in melts that are undersaturated with Ni sulphide were calculated with Eqn 3 for the Ca-enriched melt composition used for this study, using A_M values from Table 4, except for A_{Ni}, which was assumed to be 30 (Fig. 3a) and 254 (Fig. 3b), as explained above. Note that the coefficients in Table 4 give C_S in wt% whereas those in O'Neill and Mavrogenes give concentrations in ppm. The difference is accommodated by the A_0 term. Silicate melts saturated with a Ni sulphide phase should plot at the intersection between lines for undersaturated melts and the sulphide saturation line, while those that are undersaturated should plot on the thinner lines to the left of the bold NiS saturation line. The majority of group 1 points judged to be in equilibrium plot on the predicted group 1 line. A few scatter along a trend parallel to

the sulphide saturation line, and the points thought to exhibit disequilibrium scatter more widely. The group 2 points plot close to the group 2 line and within error of the NiS saturation line. No points lie at the intersection between the NiS saturation line and the undersaturated lines even though an NiS phase has been analysed from some of the samples. This is attributed to one or more errors in the assumptions upon which the calculated position of the NiS saturation line depends, which are discussed above.

The most likely explanation for the poorly equilibrated samples and the scatter of group 1 points parallel to the NiS line is that the presence of the NiS phase interferes with equilibration between the melt phase and the input gases. In this case, local oxygen and sulphur gas fugacities would be different to those that are supposed to be imposed by the gas flow apparatus. The direction of the deviation is consistent with reduced local sulphur fugacity or increased local oxygen fugacity. The former is the most likely because the formation of the NiS melt potentially affects sulphur fugacity. If the NiS melt blebs were surrounded by silicate melt during their formation, then growth of NiS blebs would require S to diffuse through the silicate melt towards the bleb. If this process was faster than diffusion of S from the gas into the melt bead, then the local S fugacity within the melt would be reduced and data would lie along the S saturation line as observed. This geometry is consistent with the observed distribution of dark material in the glass beads. There is no evidence that the formation of a Ca-rich phase, which is indicated by the low Ca contents of several of the samples, affects the Ni-S systematics, as the sulphide melt does not contain significant Ca (Table 3c).

4.1.4 Copper

The data from the Cu-bearing glasses is consistent with massive Cu loss, either to the observed Cu sulphide phase, or to a CuS vapour species. Either would limit Cu and S concentrations in the same way that the presence of a Ni sulphide melt phase affects Ni and S concentrations. An estimate of the position of the SCSS line for Cu_2S was made using equivalents of Eqns 4 to 7, and data for copper sulphide melt phase from Barin (1989) (Fig. 3c). Predicted S contents on the SCSS line are below the detection limit for all the copper contents investigated, and thus the observation that few of the samples contained detectable S is consistent with thermodynamic prediction. Cu volatilisation has been invoked to explain copper loss from natural melt inclusions (Kamentetsky and Danushevsky, 2005). Mass balance calculations would be a useful way to assess the relative importance of the two mechanisms. However, retrieval of the glass bead is often incomplete so this is not possible for the samples described here.

4.2 Geological significance of copper- and nickel-bearing sulphide melts

Sulphide melts have been shown to occur in magmatic and metamorphic ore-forming environments (e.g. Mavrogenes et al., 2001; Mungall, 2002). These melts play an important role in ore-forming processes because of their ability to concentrate and transport high concentrations of elements of economic interest, such as Ni and Cu, that occur only in trace quantities in aqueous fluids or silicate melts. The presence of sulphide melts also has the ability to fractionate chalcophile elements that are of interest for isotopic studies, such as rhenium and osmium, in ways that cannot be predicted on the basis of

existing experimental evidence.

Stabilisation of sulphide melts by Ni and Cu is of interest because only a small quantity of sulphide melt is required to effectively strip a silicate melt of S, Ni and Cu, and to change Re/Os ratios. Such a low volume melt may never be recognised in the field. However, calculations of SCSS properties may be used to assess if such a melt existed, and to predict the consequences of its segregation.

4.3 Review of predictive model for the sulphide capacity

The thermodynamic background and derivation of the model for sulphide capacity (Eqn 3) are described in detail by O'Neill and Mavrogenes (2002). However, it is useful to review the fundamental assumptions on which it is based. These are (1) that S dissolves in melts according to the Fincham-Richardson relationship; (2) that the melt can be described as a fused salt with interlocking cation and anion lattices as described by Temkin (see discussion by Moretti 2005); and (3) that interactions between the two lattices can be described with the reciprocal solution model (e.g. Wood and Nicholls, 1987).

Data from previous work (e.g. O'Neill and Mavrogenes, 2002) suggests that the Fincham-Richardson relationship holds for a wide range of melt composition. Data from this study shows that the relationship is also valid for Mn-bearing melts. Data from Ni-, Cu- and W-bearing melts does not unequivocally support Fincham-Richardson composition relationship for these metals because of saturation with a Ni-sulphide or Cu-sulphide phase, and low S concentrations under oxidising conditions, respectively. The second assumption is unlikely to

provide a good physical representation of silicate melts. Previous work (e.g. Dolejs and Baker, 2005; Mysen, 2003; Wang et al., 1995) has shown that silicate melts consist of polymeric chains of Si and Al tetrahedra, and anions such as O have been shown to be associated either with the polymers, in which case the anions are described as "bridging", or with lone cations, in which case the anions are described as "non-bridging". Additionally, the model derivation combines two slightly different definitions of the cation mole fraction, so the model is semi-empirical. These issues do not prevent the model from providing an excellent representation of S solubility across a wide range of melt compositions, however, so the utility of the model is assumed to be unaffected by these issues. The reciprocal solution model provides a convenient and tractable way to deal with interactions between the notional cation and anion lattices and is well suited for the task. The O'Neill and Mavrogenes (2002) model would therefore be expected to be suitable for extension to the Mn-, and W-bearing systems investigated in this study. The model is not calibrated for the Ni- and Cu-bearing systems because the range of melt S contents is limited by the formation of a sulphide melt phase.

4.4 Fitting Procedure

First, it was necessary to check that the S analysis method used for this study produced S concentrations consistent with those used for the original calibration of the O'Neill and Mavrogenes (2002) model (OM2002). This step was deemed necessary because there have been a number of changes to the electron microprobe hardware and measurement protocols since the original measurements were made, and any systematic shift could seriously bias results. S

contents were remeasured for 34 of the O'Neill and Mavrogenes (2002) samples, and the results were compared to the original analyses. It was found that $S_{new} = 0.946\ (\pm\ 0.004)\ S_{old}$. This small but systematic shift was incorporated into the model by adjusting the A_0 parameter in Eqn 3 so that the results become directly comparable, thus $A_{0,new} = A_{0,old} + \ln 0.946 = -5.076$ for concentrations in ppm, and $A_{0,new}$ equal to -14.286 for concentrations in wt%.

The expression of O'Neill and Mavrogenes (2002) was then tested for the Ca-rich melt composition used for this study. The sulphur capacities of all samples with S $>$ 0.015 wt% and additive metal concentrations $<$ 0.05 wt % (n=28) were compared to sulphur capacities calculated with Eqn 3 (Fig. 4). Differences between the samples are attributed to variation in the CaO and FeO content of the samples. Results (Fig. 4) show that the O'Neill and Mavrogenes (2002) expression predicts the low sulphur capacity samples well but underestimates the sulphur capacity for high sulphur capacity melts from this dataset. The main difference between the low and high sulphur capacity melts is the calcium content, so investigations of the discrepancy focussed on this term.

The low additive metal subset of the data was regressed to obtain a new estimate for A_{Ca}, $A_{Ca,new}$, which gave a value for $A_{Ca,new}$ of 8.73 $\pm$ 0.09. This value is close to, but significantly different from, the original calibrated value for A_{Ca}, which is 7.56 $\pm$ 0.13. Use of the new value for A_{Ca} reproduces the high sulphur capacity part of the dataset well (Fig. 4) but overestimates sulphur capacities for the low sulphur capacity part of the dataset. This suggests that a simple linear term may be unsuitable as a descriptor for the high calcium melts used for this study, possibly because of issues with the conceptual

mixing model. However the range of compositions available is insufficient for development of an alternative model so the original format is retained. The normalised deviation of the data from models with A_{Ca} and $A_{\mathrm{Ca,new}}$ were 29 and 11% respectively. However, the advantages of this improvement in fit were outweighed by the disadvantages associated with the introduction of a new ad-hoc value for the calibration parameter that is valid only in a restricted range of melt composition, so the old value for A_{Ca} was retained.

Data for Mn- and W-bearing glasses were then fit to Eqn 3 to determine A_{Mn} and A_{W}. Data for B180906, which was run at conditions sufficiently oxidising that significant sulphate would be expected in the melt (Moretti, pers. comm.) was excluded from the fit because the OM2002 model is for sulphur as sulphide. Values for the other coefficients were those of O'Neill and Mavrogenes (2002), with A_0 adjusted to account for bias in S analyses relative to the earlier study (Table 4) and the use of the wt% concentration scale. Mole fractions used in the fitting routine were single cation mole fractions, e.g.,

$$X_{\mathrm{Al}} = \frac{\frac{c_{\mathrm{Al}}}{26.98}}{\frac{c_{\mathrm{Si}}}{28.09} + \frac{c_{\mathrm{Al}}}{26.98} + \frac{c_{\mathrm{Fe}}}{55.85} + \frac{c_{\mathrm{Mg}}}{24.3} + \frac{c_{\mathrm{Ca}}}{40.08}} \tag{8}$$

where c_i is the wt % of element i. The data for Mn fit well (Fig 5a), in spite of the issues with A_{Ca}, to give a value for A_{Mn} of 29.5 $\pm$ 1.7. This value is similar to that obtained by O'Neill and Mavrogenes (2002) for Fe. The systematic deviation of the low Mn samples from the 1:1 fit line is attributed to the issues with the value for A_{Ca}.

The high W and low W data coalesce once variation with Ca content of the melt is taken into account, and the data for also fit well to the model (Fig 5b), with a value for A_{W} of 8.5 $\pm$ 6.9. χ^2 for the fit is 16.6 (n=18), which indicates

that the model describes the data at an acceptable level. The low value of A_W, which is within error of zero, is consistent with the negligible effect of W on S solubility. There is, therefore, little evidence of any preference for W-S neighbours within the melt. Note that χ^2 is only usable as a fit diagnostic for data sets that only include one set of oxygen and sulphur fugacities. This is because the uncertainties depend on fugacities, so data sets with more than one set of conditions do not have gaussian distribution of uncertainties, which invalidates the use of the χ^2 statistic.

The Ni-bearing data was not fit because the sulphide capacity is insensitive to the precise value of A_{Ni} in the concentration range accessed by this study (Fig. 3).

4.5 Use of model for prediction

Run B270306 was not included in the fitting process, so it can be used as a test for the model. This run included melt compositions far from the ADeu + Ca composition that was used for the calibration (Table 3a), plus Mn at a concentration of 3.5 wt %. Sulphide capacities for these samples were predicted with a version of Eqn (3) that includes the calibrated value of A_{Mn}. Predicted values of C_S are compared with the observed values in Fig 6. The observed and predicted values agree well with a χ^2 for the comparison of 5.2 (n=6).

The model is not suitable, in its present form, for prediction of natural data because there is no provision for variation in temperature and pressure away from the conditions of 1400 °C and 1 bar that were used for the experiment. Further work is needed to determine the pressure and temperature dependence

of Eqn (3).

4.6 Comparison with other models

There are a number of other models available for the calculation of the S content of silicate melts (e.g. Moretti and Ottonello, 2005; Scaillet and Pichavant, 2005; Wallace and Carmichael 1992). The majority of these models are derived more empirically than the model used here, and so, although they reproduce their calibration data well, they might be expected to perform less effectively when extrapolated to conditions other than those of calibration. Three of these models are considered here; results are summarised in Table 5.

The model of Wallace and Carmichael (1992) is similar in many ways to the O'Neill and Mavrogenes (2002) model, in that it includes a similar composition relationships and a dependence on $\ln fS_2$ and $\ln fO_2$, with exponents of opposite sign for fS_2 and fO_2. The main differences are that the coefficients of the $\ln fS_2/fO_2$ dependence are different to 0.5, that is, it is inconsistent with the Fincham-Richardson relationship, and that it includes additional terms in $\ln X_{FeO}$ and $1/T$. The model was applied to the Mn data from this study with the adjustment that X_{FeO} for the model input was equal to $X_{FeO} + X_{MnO}$ from the experimental data. This is justified in view of the similar effects that these elements have on S solubility. The mean and standard deviation of the residuals of the model predictions (Fig. 7a) relative to the experimental data are 0.014 and 0.162 wt% respectively. The mean is within error of zero, which suggests that there is no significant systematic deviation of the data from the model. The standard deviation of the residuals is significantly higher than the analytical standard deviation (0.015 wt%). Some of the discrepancy is ac-

counted for by additional uncertainties in the model, such as those associated with $\ln f O_2$ and $\ln f S_2$ but the large size of the standard deviation suggests that the model does not replicate the data particularly well.

The model of Scaillet and Pichavant (2005) is also similar to the O'Neill and Mavrogenes (2002) model in that it incorporates a similar set of compositional terms. However, it differs in that it accounts for changes in oxygen and S fugacity via a set of empirical terms in different powers of ΔNNO and ΔFFS, which measure the deviation of the experimental values for Log $f O_2$ and Log $f S_2$ from the Ni-NiO and Fe-FeS buffers respectively. This model was calibrated using the O'Neill and Mavrogenes (2002) data so it might be expected to perform well on the the data from this study. The model performs well at sulphur contents less than 0.2 wt% (Fig. 7b) but mostly underpredicts at higher sulphur concentrations. The mean and standard deviation of the residuals are -0.085 and 0.144 wt% respectively; the standard deviation is again much larger than the expected analytical uncertainty.

Fig. 7c shows the performance of the OM2002 model for the Mn data; the model underpredicts the low Mn data and overpredicts the high Mn data, which is partly due to the issues with the A_{Ca} term discussed in section 4.4. The mean and standard deviation of the residuals are -0.016 and 0.185 respectively. The mean is relatively low, as would be expected given that the model was calibrated using the data shown, but the standard deviation is relatively high at 0.185 wt%, which is, again, significantly higher than the analytical uncertainty, and reflects the systematic underprediction of sulphur in the low sulphur samples and the scatter of the samples with the highest sulphur concentrations.

642 The model of Moretti and Ottonello (2005) (MO2005) combines a set of com-
643 position dependent terms of similar form to those in Eqn 3 but with additional
644 pressure and temperature dependencies, a term to account for the effect of dif-
645 ferent degrees of polymerisation on the anion lattice, and a term that includes
646 the standard state fugacities of sulphur and oxygen. This expression is de-
647 rived and calibrated to deal with an extensive range of melt compositions and
648 pressure-temperature conditions. Both sulphide and sulphate species in the
649 melt are accounted for, so this model can be applied over a much wider range
650 of oxidation states than those described above. Application of this model to
651 the data from this study (Fig. 7d) shows that the model copes well with the
652 high Ca bulk composition although there is a systematic underprediction of
653 sulphur contents at the higher S contents produced by this study. The model
654 performs particularly well on the high Mn, low Ca points that are outliers
655 in both the Scaillet and Pichavant and OM2002 model predictions, and on
656 the scatter in the high sulphur points that are over-predicted by OM2002.
657 This is attributed to the use of terms that account for polymerisation on the
658 anion lattice. Significant sulphate concentrations in the melt ($> 3\%$) are not
659 predicted for any of the samples with sulphur contents above the detection
660 limit, although sulphur in the most oxidised run, B180906, is predicted to be
661 all sulphate. However, it is difficult to assess the success of the MO2005 model
662 with the B180906 data because sulphur contents in these samples are below
663 the detection limit. The mean and standard deviation of the residuals for this
664 model are 0.044 and 0.098 wt% respectively; this is the lowest value for the
665 standard deviation of the four models and reflects the tight grouping of the
666 points in Fig. 7d.

667 It is interesting to compare the values of the calibration parameters for the

OM2002 model with those of MO2005, as parameters in both models have related thermodynamic meanings. Comparison of the model derivations provides the expression

$$\ln \frac{K'_{\mathrm{O-S,Fe}}}{K'_{\mathrm{O-S,Mn}}} = A_{\mathrm{Fe}} - A_{\mathrm{Mn}} \tag{9}$$

where $K'_{\mathrm{O-S,M}}$ is the equilibrium constant for the reaction

$$M_{2/v}\mathrm{O}_{\mathrm{melt}} + 0.5\mathrm{S}_{2,\mathrm{gas}} = M_{2/v}\mathrm{S}_{\mathrm{melt}} + 0.5\mathrm{O}_{2,\mathrm{gas}} \tag{10}$$

where v is the charge on cation M. Values for $\ln \frac{K'_{\mathrm{O-S,Fe}}}{K'_{\mathrm{O-S,Mn}}}$ calculated from the data compilation in Ottonello and Moretti (2005) range from +5 to -5, depending on the data source, which is consistent with values for $A_{\mathrm{Fe}} - A_{\mathrm{Mn}}$ of -3±2 from this study and OM2002. The final calibrated value for $\ln \frac{K'_{\mathrm{O-S,Fe}}}{K'_{\mathrm{O-S,Mn}}}$ from OM2005 is consistent with an $A_{\mathrm{Fe}} - A_{\mathrm{Mn}}$ of +5, which is at an extreme end of the proposed range. Both sets of parameters fit the same data well, so discrepancies in absolute values are attributed to the effects of correlated parameters in data-set fitting process, which are accentuated by the relatively restricted range of composition space for which experimental data are available. The implication of this observation is that it may be unwise to infer thermodynamic data for melt components directly from such calibrations.

5 Conclusions

The presence of Mn in silicate melts enhances S solubility, with S contents of up to 1 wt % in Mn-rich melts (up to 10 wt % Mn). Experiments performed at different fO_2 and fS_2 conditions show that S solubility is consistent with the Fincham-Richardson relationship. W-bearing melts did not show

any significant correlation between S and W concentrations. S concentrations in W-bearing experiments at higher fO_2 values were below detection limits, so it was not possible to investigate the validity of the Fincham-Richardson relationship for these samples.

Ni- and Cu-bearing melt experiments resulted in the formation of an immiscible metal sulphide phase over a wide range of fO_2, fS_2, and metal concentrations. This result is consistent with thermodynamic predictions of sulphide melt phase stability. Results for Ni are also consistent with local reductions in fS_2 caused by rates of S transfer between gas and melt that are slower than the rate of diffusion of S within the melt. The formation of Ni- and Cu-bearing sulphide melt phases at low S concentrations (<0.2 wt% for Ni and <0.015 wt% for Cu) shows that these elements stabilise, and are likely to fractionate into, a sulphide melt phase, with implications for ore-forming processes and the fractionation of other chalcophile elements via sulphide melts.

The model of O'Neill and Mavrogenes (2002) for prediction of S solubility in silicate melts was calibrated for the Mn-, and W-bearing systems investigated here. The A_M coefficients for Mn, Ni and W are 29.5 $\pm$ 1.7 and 8.5 $\pm$ 6.9 respectively. The physical implications of the model are that Mn-S nearest neighbours are thermodynamically favoured and thus relatively common in the melt, whereas W-S nearest neighbours will occur only in proportions determined by the products of their concentrations.

Alternative expressions for the calculation of S content in melts were tested on the Mn-bearing data from this study, under the assumption that Mn behaves identically to Fe. Results from the models of Scaillet and Pichavant (2005) and Wallace and Carmichael (1992) reproduced the data reasonably well, in spite

of the fact that these models incorporate very different functional relationships between S content, fO_2 and fS_2. The model of Moretti and Ottonello performed exceptionally well, and reproduced features of the data that were not well modelled by the other techniques, including that of OM2002. This is attributed to consideration, in their model, of mixing on the anion lattice.

The extended expression of O'Neill and Mavrogenes (2002) was tested on Mn-bearing melts of compositions quite different to that of the original calibration. The expression performed well on these melts, which demonstrates the versatility and utility of the expression for the prediction of the solubility of S in silicate melts.

6 Acknowledgements

Experimental assistance from Dean Scott and Rikki Bailey are gratefully acknowledged. KE was supported by an Australian Synchrotron Research Program Fellowship, which is funded by the Commonwealth of Australia under the Major National Research Facilities Program. Roberto Moretti is thanked for a thoughtful review and provision of the OM2005 modelled values for the experimental data set. Two anonymous reviewers are also thanked for detailed reviews.

References

Alt, J.C., Shanks, W.C. and Jackson, M.C., 1993. Cycling of sulfur in subduction zones - the geochemistry of sulfur in the Mariana-island arc and back-arc trough. Earth and Planetary Science Letters, 119(4): 477-494.

737 Barin, I., Sauert, F., Schultze-Rhonhof, E. and Sheng, W.S., 1989. Thermo-
738 chemical data of pure substances, Parts I and II. Weinheim, VCH, 1939
739 pp.
740 Buchanan, D.L. and Nolan, J., 1979. Solubility of sulfur and sulfide immisci-
741 bility in synthetic tholeiitic melts and their relevance to Bushveld-complex
742 rocks. Canadian Mineralogist, 17: 483-494.
743 Buchanan, D.L., Nolan, J., Wilkinson, N. and de Villiers, J.P.R., 1983. An
744 experimental investigation of sulhur solubility as a function of temperature
745 in synthetic silicate melts. Geological Society of South Africa Special Pub-
746 lication, 7: 383-391.
747 Cawthorn, R.G., 2005. Contrasting sulphide contents of the Bushveld and
748 Sudbury Igneous Complexes. Mineralium Deposita, 40(1): 1-12.
749 Clemente, B., Scaillet, B. and Pichavant, M., 2004. The solubility of sulphur
750 in hydrous rhyolitic melts. Journal of Petrology, 45(11): 2171-2196.
751 de Hoog, J.C.M., Hattori, K.H. and Hoblitt, R.P., 2004. Oxidized sulfur-rich
752 mafic magma at Mount Pinatubo, Philippines. Contributions to Mineralogy
753 and Petrology, 146(6): 750-761.
754 de Hoog, J.C.M., Mason, P.R.D. and van Bergen, M.J., 2001. Sulfur and
755 chalcophile elements in subduction zones: Constraints from a laser abla-
756 tion ICP-MS study of melt inclusions from Galunggung Volcano, Indonesia.
757 Geochimica et Cosmochimica Acta, 65(18): 3147-3164.
758 Dixon, J.E., Clague, D.A. and Stolper, E.M., 1991. Degassing history of wa-
759 ter, sulfur, and carbon in submarine lavas from Kilauea volcano, Hawaii.
760 Journal of Geology, 99(3): 371-394.
761 Dolejs, D. and Baker, D.R., 2005. Thermodynamic modeling of melts in
762 the system Na_2O-$NaAlO_2$-SiO_2-F_2O-1. Geochimica Et Cosmochimica Acta,
763 69(23): 5537-5556.

764 Eggins, S.M., Rudnick, R.L. and McDonough, W.F., 1998. The composition
765 of peridotites and their minerals: a laser-ablation ICP-Ms study. Earth and
766 Planetary Science Letters, 154: 53-71.
767 Fincham, C.J.B. and Richardson, F.D., 1954. The behaviour of sulphur in
768 silicate and aluminate melts. Proceedings of the Royal Society of London.
769 Series A, 223: 40-62.
770 Fischer, T.P., Giggenbach, W.F., Sano, Y. and Williams, S.N., 1998. Fluxes
771 and sources of volatiles discharged from Kudryavy, a subduction zone vol-
772 cano, Kurile Islands. Earth and Planetary Science Letters, 160(1-2): 81-96.
773 Haughton, D.R., Roeder, P.L. and Skinner, B.J., 1974. Solubility of sulfur in
774 mafic magmas. Economic Geology, 69(4): 451-467.
775 Jarosewich, E., Nelen, J.A. and Norberg, J.A., 1979. Electron microprobe
776 reference samples for mineral analyses. Smithsonian Contributions to Earth
777 Sciences, 20: 68-72.
778 Jugo, P.J., Luth, R.W. and Richards, J.P., 2005. An experimental study of
779 the sulfur content in basaltic melts saturated with immiscible sulfide or
780 sulfate liquids at 1300 degrees C and 1 GPa. Journal of Petrology, 46(4):
781 783-798.
782 Kamenetsky, V.S. and Danyushevsky, L.V., 2005. Metals in quartz-hosted
783 melt inclusions: Natural facts and experimental artifacts. American Miner-
784 alogist, 90(10): 1674-1678.
785 Katsura, T. and Nagashim.S, 1974. Solubility of sulfur in some magmas at 1
786 atmosphere. Geochimica et Cosmochimica Acta, 38(4): 517-531.
787 Mavrogenes, J.A., MacIntosh, I.W. and Ellis, D.J., 2001. Partial melting of
788 the Broken Hill galena-sphalerite ore: Experimental studies in the system
789 PbS-FeS-ZnS-(Ag_2S). Economic Geology and the Bulletin of the Society of
790 Economic Geologists, 96(1): 205-210.

Moretti, R., 2005. Polymerisation, basicity, oxidation state and their role in ionic modelling of silicate melts. Annals of Geophysics, 48(4-5): 583-608.

Moretti, R. and Ottonello, G., 2005. Solubility and speciation of sulfur in silicate melts: The Conjugated Toop-Samis-Flood-Grjotheim (CTSFG) model. Geochimica Et Cosmochimica Acta, 69(4): 801-823.

Mungall, J.E., 2002. Late-stage sulfide liquid mobility in the main mass of the Sudbury Igneous Complex: Examples from the Victor Deep, McCreedy East, and Trillabelle deposits. Economic Geology and the Bulletin of the Society of Economic Geologists, 97(7): 1563-1576.

Nilsson, K. and Peach, C.L., 1993. Sulfur speciation, oxidation-state, and sulfur concentration in backarc magmas. Geochimica et Cosmochimica Acta, 57(15): 3807-3813.

O'Neill, H.S.C. and Eggins, S.M., 2002. The effect of melt composition on trace element partitioning: an experimental investigation of the activity coefficients of FeO, NiO, CoO, MoO_2 and MoO_3 in silicate melts. Chemical Geology, 186(1-2): 151-181.

O'Neill, H.S.C. and Mavrogenes, J.A., 2002. The sulfide capacity and the sulfur content at sulfide saturation of silicate melts at 1400 degrees C and 1 bar. Journal of Petrology, 43(6): 1049-1087.

Pearce, N.J.G. et al., 1997. A compilation of new and published major and trace element data for NIST SRM 610 and NIST SRM 612 glass reference materials. Geostandards Newsletter-the Journal of Geostandards and Geoanalysis, 21(1): 115-144.

Pina, R. et al., 2006. Petrology and geochemistry of mafic-ultramafic fragments from the Aguablanca Ni-Cu ore breccia, southwest Spain. Economic Geology, 101(4): 865-881.

Poulson, S.R. and Ohmoto, H., 1990. An evaluation of the solubility of sul-

fide sulfur in silicate melts from experimental-data and natural samples. Chemical Geology, 85(1-2): 57-75.

Scaillet, B. and Pichavant, M., 2005. A model of sulphur solubility for hydrous mafic melts: application to the determination of magmatic fluid compositions of Italian volcanoes. Annals of Geophysics, 48(4-5): 671-698.

Seo, J.D. and Kim, S.H., 1999. The sulphide capacity of CaO-SiO_2-Al_2O_3-MgO(-FeO) smelting reduction slags. Steel Research, 70(6): 203-208.

Shankar, A., Gornerup, M., Lahiri, A.K. and Seetharaman, S., 2006. Sulfide capacity of high alumina blast furnace slags. Metallurgical and Materials Transactions B-Process Metallurgy and Materials Processing Science, 37(6): 941-947.

Shima, H. and Naldrett, A.J., 1975. Solubility of sulfur in an ultramafic melt and relevance of system Fe-S-O. Economic Geology, 70(5): 960-967.

Thordarson, T., Self, S., Oskarsson, N. and Hulsebosch, T., 1996. Sulfur, chlorine, and fluorine degassing and atmospheric loading by the 1783-1784 AD Laki (Skaftar fires) eruption in Iceland. Bulletin of Volcanology, 58(2-3): 205-225.

Wallace, P. and Carmichael, I.S.E., 1992. Sulfur in basaltic magmas. Geochimica et Cosmochimica Acta, 56(5): 1863-1874.

Wang, C.Y. and Zhou, M.F., 2006. Genesis of the Permian Baimazhai magmatic Ni-Cu-(PGE) sulfide deposit, Yunnan, SW China. Mineralium Deposita, 41(8): 771-783.

Wang, Z.F., Cooney, T.F. and Sharma, S.K., 1995. In-situ structural investigation of iron-containing silicate liquids and glasses. Geochimica et Cosmochimica Acta, 59(8): 1571-1577.

Wood, B.J. and Nicholls, J., 1978. Thermodynamic properties of reciprocal solid-solutions. Contributions to Mineralogy and Petrology, 66(4): 389-400.

Young, R.W., Duffy, J.A., Hassall, G.J. and Xu, Z., 1992. Use of optical basicity concept for determining phosphorus and sulfur slag metal partitions. Ironmaking and Steelmaking, 19(3): 201-219.

Figure captions

Figure 1. Log of concentrations, in wt%, of S and metals for (a) Mn-bearing melt experiments (b) W-bearing melt experiments (c) Ni-bearing melt experiments and (d) Cu-bearing melt experiments. Error bars are for an uncertainty on the probe-derived S concentration of 0.015 wt% and uncertainties on the additive metals of 0.01wt% for Mn and Cu, 0.005wt% for Ni and 0.015wt% for W. Where error bars are not visible the propagated uncertainty is smaller than the symbol.

Figure 2. Relationship between log of sulphide capacities (wt%) and metal concentrations (wt%) for (a) Mn-bearing melts; (b) W-bearing high Ca melts; (c) W-bearing low Ca melts and (d) Ni-bearing melts Error bars are propagated assuming an uncertainty on the probe-derived S concentration of 0.15 wt% and uncertainties on the imposed fO_2 and fS_2 of 0.05 log units.

Figure 3. (a) Plot of $\frac{1}{2}\log f_{S_2} - \log[\mathrm{S, wt\%}]$ against $\frac{1}{2}\log f_{O_2}$. If the Fincham-Richardson relationship holds then the slope of the data should be 1. Line with unit slope is also shown for comparison. (b) Schematic of predicted metal-S concentration relationships where metal and S concentrations are limited by the presence of an immiscible metal sulphide phase (thick black lines). (a) Ni-S. Thin lines plot the Ni-S concentration relationships assuming that the Fincham-Richardson relationship holds and that Ni enhances S solubility in

a similar way to Fe. A_{Ni} equal to 30. This is similar to A_{Fe} which is 26.4. (b) Ni-S. Thin lines plot the Ni-S concentration relationships assuming that the Fincham-Richardson relationship holds and that Ni enhances S solubility in a similar way to Fe.A_{Ni} equal to 254. This value is used to assess the sensitivity of calculated values to A_{Ni}. The low Ni portions of the two diagrams are similar for the two different values; (c) Position of calculated SCSS for Cu_2S-bearing melt compared to S detection limit. Predicted sulphur contents are never higher than the detection limit for these samples.

Figure 4. Comparison of observed and predicted sulphide capacities for the Mn-, W- and Ni-bearing samples with additive metal content less than 0.05 wt%. Low predicted values for the model of O'Neill and Mavrogenes (2002) (closed squares) are attributed to a slightly low value for A_{Ca}.

Figure 5. Comparison of observed sulphide capacities with values calculated with the extended model of O'Neill and Mavrogenes (2002) for (a) the Mn-bearing melts (b) the W-bearing melts. The experimental data scatters close to the 1:1 line.

Figure 6. Comparison of observed and predicted sulphide capacities for samples that were not included in the calibration.

Figure 7. Comparison of observed sulphide capacities for the Mn-bearing melts with those predicted by (a) Wallace and Carmichael (1992) and (b) Scaillet and Pichavant (2005); (c) O'Neill and Mavrogenes (2002) and (d) Moretti and Ottonello (2005). Calculations were made assuming that Mn behaves identically to Fe in the first two models.

Tables

Table 1: Summary of experimental runs

Run	Metal	Concentrations	Log fO_2	Log fS_2	Log fSO_2
B231205	Ni	low	-9.6	-1.91	-3.06
B301205	W	low	-9.6	-1.91	-3.06
B030106	Mn	low	-9.6	-1.91	-3.06
B040106	Cu	low	-8.09	-1.91	-1.56
B210306	Cu	high	-8.09	-1.91	-1.56
B220306	Ni	high	-9.6	-1.91	-3.06
B230306	Mn	high	-9.6	-1.91	-3.06
B240306	W	high	-9.6	-1.91	-3.06
B050406	Mn	high	-9.6	-1.91	-3.06
B070406	Ni	10-30wt%	-9.6	-1.91	-3.06
B100406	Mn	high	-9.6	-1.91	-3.06
B110406	Mn	high	-7.18	-1.85	-0.61
B120406	Ni	high	-7.18	-1.85	-0.61
B310706	Mn	high	-9.6	-1.91	-3.06
B010806	Ni	low	-9.6	-1.91	-3.06
B020806	Mn	high	-7.18	-1.85	-0.61
B030806	Ni	low	-7.18	-1.85	-0.61
B220806	W	high	-9.6	-1.91	-3.06
B230806	W	high	-7.18	-1.85	-0.61
B140906	Ni	low	-9.6	-1.91	-3.06
B150906	W	low	-9.6	-1.91	-3.06
B180906	Mn	high	-3.09	-11.88	-1.52
B190906	Ni	high	-3.09	-11.88	-1.52
B200906	W	high	-3.09	-11.88	-1.52

Table 1: Summary of experimental runs continued

Run	Metal	Concentration	Log fO_2	Log fS_2	LogfSO_2
B111006	Mn	low	-7.59	-2.8	-1.5
B191006	Ni	low	-7.59	-2.8	-1.5
B261006	W	low	-7.59	-2.8	-1.5
B141106	W	high	-9.6	-1.91	-3.06
B151106	Mn	low	-9.6	-1.91	-3.06
B270306	Mn	3.5wt%	-9.6	-1.91	-3.06

Nominal additive contents for low concentration range samples: 0, 0.2, 0.4, 0.6, 0.8 and 1.0 wt%

Nominal additive contents for high concentration range samples: 0, 2, 4, 6, 8 and 10 wt%

All runs except B270306 use ADeu+Ca melt composition.

The ADeu+Ca composition is Si: 19.7%; Al: 6.9%; Mg: 5.3 %; Ca: 25.0%

B270306 uses a variety of CAS/MAS compositions: see Table 3a

Table 2: Summary of gas flow rates and fugacities

	CO (SCCM)	CO_2 (SCCM)	SO_2 (SCCM)	Log fO_2	Log fS_2	Log fSO_2
Group 1	80	17	3	-9.6	-1.91	-3.06
Group 2	20	59.6	30	-7.18	-1.81	-0.61
Group 3	20	59.6	3	-7.6	-2.8	-1.50
Group 4	0	97	3	-3.09	-11.88	-1.52
Copper	0	97	3	-8.1	-1.91	-1.56
SCCM: Gas flow rates in standard centimetres cubed per minute						

Table 3a: Results for Mn-bearing runs

Sample	Si (wt%)	Al(wt%)	Mg(wt%)	Ca(wt%)	Fe(wt%)	S (wt%)	Mn(wt%)	O(wt%)	Total (wt%)	Group	Appeara
B030106p1	19.63(6)	6.52(6)	5.02(5)	24.32(2)	0.895(6)	0.2651(7)	0.993(3)	42.0(1)	99.6(3)	Group 1	n.a.
B030106p2	19.93(8)	6.64(4)	5.07(3)	24.54(5)	0.73(1)	0.224(1)	0.381(3)	42.31(1)	99.9(2)	Group 1	n.a.
B030106p3	20.12(4)	6.83(3)	5.17(1)	24.78(5)	0.618(3)	0.19(2)	bdl	42.66(4)	100.38(9)	Group 1	n.a.
B030106p4	19.88(6)	6.65(3)	5.10(4)	24.695(8)	0.594(6)	0.207(2)	0.2286(2)	42.2(1)	99.6(2)	Group 1	n.a.
B030106p5	19.96(6)	6.77(3)	5.17(4)	24.75(3)	0.606(7)	0.209(2)	0.236(3)	42.50(8)	100.2(2)	Group 1	n.a.
B030106p6	19.65(8)	6.61(2)	5.07(3)	24.45(3)	0.86(1)	0.251(5)	0.755(2)	42.09(9)	99.8(2)	Group 1	n.a.
B230306p1	18.0(1)	6.65(6)	4.98(6)	22.7(1)	0.040(4)	0.68(1)	6.59(4)	41.3(2)	101.0(5)	Group 1	n.a.
∗B230306p2	19.0(2)	7.07(5)	5.3(1)	24.61(8)	0.15(2)	0.25(3)	1.26(1)	42.0(3)	99.7(6)	Group 1	n.a.
B230306p3	18.7(6)	6.9(1)	5.2(1)	23.7(4)	0.113(8)	0.322(8)	2.51(7)	41.5(1)	99.(2)	Group 1	n.a.
B230306p4	17.2(1)	6.32(8)	4.85(5)	22.1(2)	0.06(1)	0.914(7)	8.49(6)	40.6(3)	100.6(7)	Group 1	n.a.
B230306p5	19.4(8)	7.2(2)	5.6(2)	14.3(7)	0.016(2)	0.377(4)	10.0(1)	41.(1)	98.(3)	Group 1	S
B230306p6	18.17(9)	6.74(6)	5.05(4)	23.4(1)	0.09(2)	0.469(3)	4.52(3)	41.2(1)	99.7(3)	Group 1	n.a.
∗B230306p11	17.1(5)	6.4(2)	4.8(1)	21.(1)	0.035(7)	0.7(1)	6.(2)	39.(2)	95.(5)	Group 1	n.a.
B230306p12	16.9(5)	6.3(2)	4.76(1)	20.(1)	0.04(2)	0.85(3)	7.4(4)	39.(1)	96.(4)	Group 1	n.a.
B050406p1	17.1(2)	6.4(3)	4.8(2)	22.36(8)	bdl	0.801(5)	8.22(6)	40.5(4)	100.2(1)	Group 1	BS
B050406p2	19.2(8)	7.5(1)	5.8(2)	14.5(3)	bdl	0.323(6)	9.6(3)	41.(1)	98.(3)	Group 1	BS, V
B100406p3	17.2(2)	6.57(3)	4.98(8)	21.5(1)	bdl	0.916(4)	9.63(4)	41.0(2)	101.8(5)	Group 1	BS
B100406p6	19.34(8)	7.13(8)	5.40(5)	24.60(3)	0.02(1)	0.289(4)	2.27(1)	42.7(2)	101.8(3)	Group 1	BS

Figure in brackets is 1 standard deviation on the final digit

BS: Black specks; V: Vesicles; n.a. not available

Table 3a: Results for Mn-bearing runs, continued

Sample	Si(wt%)	Al(wt%)	Mg(wt%)	Ca(wt%)	Fe(wt%)	S(wt%)	Mn(wt%)	O(wt%)	Total (wt%)	Group	Appearance
B110406p1	19.3(1)	6.9(2)	5.28(1)	25.0(2)	bdl	0.023(4)	1.13(2)	41.9(2)	99.6(5)	Group 2	BS
B110406p2	18.5(3)	6.6(2)	5.0(1)	24.0(3)	bdl	0.043(4)	3.99(6)	41.2(4)	99.5(8)	Group 2	BS,V
B110406p3	18.0(3)	6.5(2)	5.0(1)	23.2(2)	bdl	0.061(4)	6.2(1)	40.8(4)	99.8(8)	Group 2	BS
B110406p4	18.1(8)	6.7(3)	5.0(2)	23.(1)	bdl	0.06(4)	6.(4)	40.9(8)	99.9(5)	Group 2	
B110406p5	18.(1)	6.5(2)	5.0(2)	24.(1)	bdl	0.05(2)	5.(3)	41.(1)	99.(1)	Group 2	BS,V
B110406p6	17.7(1)	6.12(7)	4.78(6)	23.09(6)	0.02(2)	0.072(4)	7.29(2)	40.2(2)	99.4(4)	Group 2	BS
B310706p1	20.3(1)	6.98(6)	5.43(5)	25.32(9)	0.018(1)	0.196(3)	bdl	43.2(2)	101.5(5)	Group 1	BS,V
B310706p2	19.5(1)	6.91(2)	5.35(7)	24.91(1)	0.04(2)	0.332(3)	2.07(2)	42.8(1)	102.0(2)	Group 1	BS
B310706p3	18.9(2)	6.58(9)	5.17(7)	24.2(2)	0.043(9)	0.480(2)	3.74(5)	42.0(4)	101.1(8)	Group 1	BS
B310706p4	18.4(1)	6.44(2)	5.06(2)	23.71(7)	0.05(1)	0.726(6)	6.03(2)	42.0(1)	102.4(2)	Group 1	BS, V
B310706p5	18.2(1)	6.3(1)	4.87(7)	23.24(7)	0.07(3)	0.879(4)	7.15(2)	41.8(1)	102.5(3)	Group 1	BS,V
B310706p6	17.6(2)	6.10(9)	4.76(7)	22.36(6)	0.06(2)	1.117(8)	8.74(3)	41.2(2)	102.0(4)	Group 1	BS
B020806p1	17.6(2)	6.19(3)	4.75(1)	22.62(5)	bdl	0.088(3)	9.008(1)	40.5(2)	100.8(4)	Group 2	
B020806p2	18.40(5)	6.39(2)	4.993(3)	23.76(8)	0.02(2)	0.053(2)	6.10(3)	41.25(9)	101.0(2)	Group 2	
B020806p3	17.93(5)	6.3(1)	4.92(8)	23.29(3)	0.040(7)	0.12(1)	7.27(2)	40.8(2)	100.7(3)	Group 2	BS,V
B020806p4	19.4(1)	6.76(5)	5.29(9)	25.07(8)	bdl	0.024(2)	2.122(7)	42.3(2)	101.0(3)	Group 2	V
B020806p5	19.12(5)	6.69(4)	5.09(8)	24.62(6)	bdl	0.039(2)	3.902(7)	42.10(5)	101.6(1)	Group 2	
B020806p6	18.1(1)	6.3(1)	4.87(7)	23.3(1)	bdl	0.122(4)	7.24(2)	41.0(2)	101.0(4)	Group 2	BS

Figure in brackets is 1 standard deviation on the final digit

BS: Black specks; V: Vesicles

Table 3a: Results for Mn-bearing runs, continued

Sample	Si(wt%)	Al(wt%)	Mg(wt%)	Ca(wt%)	Fe(wt%)	S(wt%)	Mn(wt%)	O(wt%)	Total (wt%)	Group	Appearanc
B180906p2	18.36(9)	6.40(3)	4.92(4)	23.41(9)	bdl	bdl	6.19(2)	41.03(9)	100.5(2)	Group 4	V
B180906p3	17.5(3)	6.15(7)	4.77(2)	22.1(2)	0.02(1)	bdl	9.4(4)	40.2(4)	100.2(6)	Group 4	
B180906p4	18.2(1)	6.29(3)	4.87(1)	22.94(3)	bdl	bdl	7.35(2)	40.8(1)	100.6(2)	Group 4	BS, V
B180906p5	19.1(1)	6.61(4)	5.10(6)	24.1(1)	0.02(1)	bdl	3.944(4)	41.8(2)	100.7(4)	Group 4	V
B180906p6	19.7(1)	6.86(5)	5.2(1)	24.89(4)	bdl	bdl	2.04(1)	42.5(2)	101.3(5)	Group 4	BS
B111006p1	20.8(3)	6.1(3)	4.4(2)	25.4(3)	bdl	0.019(3)	0.77(1)	42.44(9)	100.1(3)	Group 3	BS
∗B111006p2	20.2(5)	7.6(7)	4.9(8)	24.(1)	bdl	0.019(7)	1.02(9)	43.0(3)	101.2(2)	Group 3	BS
∗B111006p4	20.(1)	6.6(7)	5.6(1)	25.(1)	0.025(4)	0.017(4)	0.33(3)	42.2(7)	99.8(5)	Group 3	BS
B111006p5	19.8(1)	6.95(7)	5.43(9)	25.2(2)	0.03(1)	0.0183(6)	0.231(2)	42.6(2)	100.4(3)	Group 3	BS
B111006p6	19.59(1)	6.89(6)	5.36(9)	25.13(9)	0.036(4)	0.017(4)	0.608(5)	42.26(3)	100.04(6)	Group 3	
B151106p1	21.08(9)	7.08(4)	5.25(2)	22.03(7)	0.048(7)	0.229(2)	0.379(5)	42.93(9)	99.1(1)	Group 1	BS
B151106p4	20.84(5)	6.95(6)	5.20(2)	21.93(6)	0.05(2)	0.274(5)	1.070(6)	42.7(1)	99.2(2)	Group 1	BS
B151106p5	21.19(4)	7.02(7)	5.22(6)	22.02(6)	0.096(8)	0.219(7)	0.235(3)	42.94(4)	99.0(1)	Group 1	BS
B151106p6	20.89(7)	6.95(3)	5.18(6)	21.82(6)	0.065(4)	0.251(4)	0.840(7)	42.62(9)	98.7(1)	Group 1	

Figure in brackets is 1 standard deviation on the final digit

BS: Black specks; V: Vesicles

Table 3a: Results for Mn-bearing runs, continued

Sample	Si(wt%)	Al(wt%)	Mg(wt%)	Ca(wt%)	Fe(wt%)	S(wt%)	Mn(wt%)	O(wt%)	Total (wt%)	Group	Appearance
B270307p1	20.82(5)	7.04(5)	5.54(3)	24.91(9)	0.051(4)	0.172(6)	0.014(2)	43.76(5)	102.3(2)	Group 1	BS
B270307p2	28.9(1)	8.86(5)	11.94(2)	0.057(4)	0.059(7)	0.029(5)	3.491(9)	49.8(2)	103.2(4)	Group 1	BS
B270307p3	32.7(2)	9.44(7)	bdl	6.55(7)	0.04(1)	0.016(3)	3.43(4)	49.4(1)	101.8(2)	Group 1	BS
B270307p4	28.7(2)	8.94(5)	12.01(2)	0.0565(9)	0.06(1)	bdl	3.48(2)	49.7(2)	103.1(4)	Group 1	BS
B270307p5	19.81(2)	10.15(4)	0.045(9)	25.52(2)	0.058(7)	0.255(5)	3.511(4)	43.12(5)	102.49(9)	Group 1	BS
B270307p6	19.24(6)	6.04(3)	0.043(6)	31.15(8)	0.07(1)	0.552(5)	3.41(1)	41.32(7)	101.8(2)	Group 1	BS

Figure in brackets is 1 standard deviation on the final digit

BS: Black specks; V: Vesicles

Table 3b: Results for W-bearing runs

Sample	Si(wt%)	Al(wt%)	Mg(wt%)	Ca(wt%)	Fe(wt%)	S(wt%)	W(wt%)	O(wt%)	Total (wt%)	Group	Appearance
B301205p1	19.83(4)	6.66(5)	5.14(8)	24.70(2)	0.399(6)	0.212(2)	0.47(1)	42.23(7)	99.7(2)	Group 1	
B301205p2	19.7(1)	6.67(5)	5.11(7)	24.93(3)	0.368(5)	0.2107(7)	0.195(5)	42.1(2)	99.3(4)	Group 1	BS
B301205p3	19.8(1)	6.65(6)	5.15(5)	24.38(2)	0.486(7)	0.208(2)	0.740(6)	42.1(2)	99.6(3)	Group 1	BS
B301205p4	19.9(1)	6.67(3)	5.15(3)	24.35(5)	0.49(1)	0.208(2)	0.738(1)	42.3(1)	99.9(2)	Group 1	
B301205p5	19.82(6)	6.78(5)	5.18(3)	24.71(3)	0.459(8)	0.207(5)	0.320(4)	42.32(9)	99.8(2)	Group 1	
B301205p6	19.84(3)	6.67(5)	5.20(5)	24.58(3)	0.395(8)	0.207(2)	0.478(8)	42.21(5)	99.58(8)	Group 1	
B240306p1	20.60(6)	7.32(6)	5.55(1)	15.53(3)	0.06(1)	0.075(4)	7.74(4)	41.97(9)	98.9(2)	Group 1	BS
B240306p2	18.6(2)	6.90(5)	5.17(8)	24.89(2)	0.09(2)	0.188(3)	0.647(9)	41.1(3)	97.6(5)	Group 1	n.a.
B240306p3	22.77(4)	7.98(6)	6.2(1)	16.44(9)	0.05(2)	0.060(5)	2.21(3)	44.3(1)	100.1(3)	Group 1	n.a.
B240306p3a	22.2(1)	8.19(7)	6.19(8)	16.29(3)	0.070(1)	0.064(3)	1.09(1)	43.6(2)	97.7(4)	Group 1	BS
B240306p4	20.8(1)	7.32(6)	5.85(6)	15.51(4)	0.05(2)	0.068(2)	6.07(4)	41.9(2)	97.6(5)	Group 1	BS
∗B240306p5	22.2(1)	7.70(3)	6.05(8)	16.21(4)	0.04(1)	0.067(3)	4.11(3)	43.8(2)	100.2(4)	Group 1	BS
B240306p6	20.2(3)	7.2(2)	5.59(6)	15.0(1)	0.07(3)	0.082(5)	9.05(8)	41.6(5)	98.8(8)	Group 1	BS
∗B220806p1	22.2(3)	7.8(1)	5.9(1)	16.43(3)	bdl	0.02(2)	4.23(8)	43.9(5)	101.(1)	Group 1	BS
B220806p2	21.59(1)	7.63(9)	5.80(5)	16.03(5)	0.048(1)	0.064(4)	5.86(4)	43.23(1)	100.3(2)	Group 1	
B220806p3	21.1(1)	7.39(7)	5.69(5)	15.50(7)	0.05(1)	0.068(7)	7.6(1)	42.6(1)	100.0(3)	Group 1	
B220806p4	23.08(5)	8.14(5)	6.14(7)	16.77(2)	0.020(7)	bdl	2.23(3)	44.92(9)	101.4(2)	Group 1	BS,V
B220806p5	22.8(2)	7.89(3)	6.09(6)	19.73(2)	0.06(2)	0.073(5)	0.223(7)	45.0(2)	101.9(4)	Group 1	BS
B220806p6	20.51(9)	7.32(7)	5.6(1)	15.1(2)	0.05(1)	0.071(3)	9.27(5)	42.1(2)	100.1(6)	Group 1	BS

Figure in brackets is 1 standard deviation on the final digit

BS: Black specks; V: Vesicles; n.a. not available

Table 3b: Results for W-bearing runs, continued

Sample	Si(wt%)	Al(wt%)	Mg(wt%)	Ca(wt%)	Fe(wt%)	S(wt%)	W(wt%)	O(wt%)	Total (wt%)	Group	Appearance
B230806p1	20.7(1)	7.32(1)	5.7(1)	15.46(8)	bdl	bdl	8.19(5)	42.2(1)	99.6(3)	Group 2	V
B230806p2	21.5(2)	7.55(1)	5.9(1)	15.9(1)	bdl	bdl	6.49(4)	43.1(3)	100.5(7)	Group 2	BS, V
B230806p3	22.5(2)	7.81(8)	6.1(1)	20.1(1)	bdl	bdl	0.02(3)	44.6(4)	101.1(8)	Group 2	
B230806p4	22.13(9)	7.76(1)	6.04(7)	16.3(1)	bdl	bdl	4.27(3)	43.7(2)	100.2(4)	Group 2	BS,V
B230806p5	22.8(2)	8.00(8)	6.2(1)	16.6(1)	bdl	bdl	2.34(4)	44.4(4)	100.3(9)	Group 2	BS
B230806p6	20.1(2)	7.16(8)	5.52(8)	14.98(6)	bdl	bdl	9.88(7)	41.5(3)	99.2(6)	Group 2	BS
∗B150906p1	19.7(2)	7.0(3)	5.5(5)	25.1(3)	bdl	0.3(1)	0.70(9)	42.9(2)	101.4(4)	Group 1	
∗B150906p2	20.1(1)	6.93(6)	5.36(6)	25.1(1)	0.040(5)	0.200(3)	0.28(3)	42.9(2)	101.0(4)	Group 1	
B150906p3	19.7(1)	6.83(5)	5.39(9)	24.95(7)	0.18(2)	0.206(4)	0.89(3)	42.5(2)	100.7(3)	Group 1	
∗B150906p4	19.9(1)	6.89(6)	5.4(1)	25.14(9)	0.17(2)	0.202(5)	0.49(5)	42.7(2)	101.0(3)	Group 1	
B150906p5	21.16(3)	7.32(1)	5.80(8)	22.80(9)	0.163(7)	0.134(2)	bdl	43.7(1)	101.1(3)	Group 1	
B200906p1	17.70(9)	6.30(1)	4.84(2)	20.73(9)	bdl	bdl	10.3(3)	39.9(1)	99.8(2)	Group 4	
B200906p2	20.3(1)	7.00(6)	5.43(8)	25.32(2)	bdl	bdl	0.05(4)	43.1(1)	101.2(3)	Group 4	V
B200906p3	17.9(2)	6.37(7)	4.9(1)	21.88(6)	bdl	bdl	8.12(4)	40.2(2)	99.4(4)	Group 4	BS
B200906p4	18.8(1)	6.66(8)	5.28(5)	21.58(5)	bdl	bdl	6.53(5)	41.18(5)	100.10(8)	Group 4	V
B200906p5	19.2(1)	6.61(8)	5.31(7)	24.46(4)	bdl	bdl	2.67(4)	41.7(1)	100.0(3)	Group 4	
B200906p6	19.3(1)	6.76(5)	5.37(3)	22.44(2)	bdl	bdl	4.41(6)	41.7(2)	100.1(3)	Group 4	

Figure in brackets is 1 standard deviation on the final digit

BS: Black specks; V: Vesicles

Table 3c: Results for Ni-bearing runs

Sample	Si(wt%)	Al(wt%)	Mg(wt%)	Ca(wt%)	Fe(wt%)	S(wt%)	Ni(wt%)	O(wt%)	Total (wt%)	Group	Appearan
B231205p1	19.81(8)	6.64(2)	5.14(3)	24.96(2)	0.374(7)	0.214(2)	0.006‡	42.2(1)	99.3(2)	Group 1	BS
B231205p2	19.91(9)	6.71(2)	5.14(4)	24.85(3)	0.418(9)	0.2111(9)	0.021‡	42.3(1)	99.6(3)	Group 1	BS
B231205p3	19.84(5)	6.74(4)	5.14(4)	25.11(3)	0.345(2)	0.213(3)	0.024‡	42.34(1)	99.8(2)	Group 1	BS
B231205p4	19.8(1)	6.76(3)	5.17(4)	25.06(3)	0.34(1)	0.213(2)	0.006‡	42.3(1)	99.8(3)	Group 1	BS
B231205p5	19.8(2)	6.74(5)	5.15(7)	24.82(3)	0.521(4)	0.214(2)	0.003‡	42.3(2)	99.5(4)	Group 1	BS
B231205p6	19.9(1)	6.73(5)	5.19(5)	24.99(4)	0.494(8)	0.227(6)	0.005‡	42.4(2)	99.9(3)	Group 1	BS
B231205p7	19.87(8)	6.72(5)	5.11(4)	24.97(3)	0.338(7)	0.214(3)	0.0172(9)	42.3(1)	99.5(3)	Group 1	BS
B220306p1	22.8(5)	8.5(2)	6.44(7)	16.9(3)	0.08(3)	0.052(6)	0.026(2)	44.6(8)	99.(2)	Group 1	n.a.
B220306p2	23.2(3)	8.57(6)	6.45(9)	16.9(1)	0.12(1)	0.063(2)	0.05(2)	45.1(4)	100.5(9)	Group 1	n.a.
B220306p3	19.5(1)	7.22(9)	5.5(1)	24.63(3)	0.10(1)	0.188(5)	0.021(3)	42.3(3)	99.5(7)	Group 1	n.a.
B220306p4	22.3(2)	8.27(7)	6.34(5)	16.84(4)	0.14(1)	0.064(2)	0.032(2)	43.8(3)	97.9(6)	Group 1	BS
B220306p5	21.(3)	7.7(1)	5.9(7)	21.(6)	0.09(7)	0.12(9)	0.0304(3)	43.(2)	98.2(4)	Group 1	BS
B220306p6	18.89(5)	7.01(6)	5.35(4)	24.69(1)	0.08(2)	0.176(2)	0.029(2)	41.34(1)	97.6(2)	Group 1	
NiS phase	bdl	bdl	bdl	bdl	1.46	23.93	71.25	n.a.	96.6	Group 1	
∗B070406p2	22.9(4)	8.6(2)	6.47(4)	16.90(5)	0.08(3)	bdl	0.11(2)	44.9(6)	100.(1)	Group 1	BS
B070406p4	22.86(6)	8.47(2)	6.33(1)	16.81(1)	0.062(2)	0.0529(8)	0.029(7)	44.55(1)	99.2(2)	Group 1	BS
B070406p5	22.8(2)	8.51(5)	6.42(3)	16.80(7)	0.050(4)	0.055(6)	0.033(9)	44.6(2)	99.4(5)	Group 1	BS
B070406p6	22.717(8)	8.46(6)	6.5(1)	16.89(8)	0.04(2)	0.058(5)	0.033(2)	44.50(6)	99.2(2)	Group 1	BS
NiS phase	bdl	bdl	bdl	bdl	0.32	23.83	72.78	n.a.	96.6	Group 1	

Figure in brackets is 1 standard deviation on the final digit

‡:Laser analysis, uncertainties are at the ppb level

BS: Black specks; V: Vesicles

Table 3c: Results for Ni-bearing runs, continued

Sample	Si(wt%)	Al(wt%)	Mg(wt%)	Ca(wt%)	Fe(wt%)	S(wt%)	Ni(wt%)	O(wt%)	Total (wt%)	Group	Appearance
∗B120406p1	20.1(2)	7.49(5)	5.63(3)	24.7(1)	0.04(2)	0.03(2)	0.39(5)	43.2(2)	101.6(4)	Group 2	
∗B120406p2	22.43(1)	8.43(1)	6.36(1)	16.67(5)	0.03(1)	bdl	1.1(3)	44.2(2)	99.3(6)	Group 2	BS
B120406p3	19.11(1)	7.12(7)	5.41(6)	24.91(5)	0.10(5)	0.020(5)	0.46(1)	41.8(1)	99.0(3)	Group 2	BS
B120406p4	19.7(2)	7.34(5)	5.54(4)	24.84(6)	0.05(2)	0.017(4)	0.54(1)	42.7(3)	100.9(7)	Group 2	BS
B120406p5	22.6(3)	8.39(1)	6.31(9)	16.50(7)	0.056(3)	bdl	1.01(4)	44.3(3)	99.3(6)	Group 2	
B120406p6	18.7(9)	6.9(3)	5.3(2)	24.6(2)	0.02(2)	0.022(3)	0.312(9)	41.(1)	97.(3)	Group 2	BS
B120406p6a	23.69(6)	8.73(9)	6.55(3)	16.68(6)	0.018(1)	bdl	0.450(3)	45.87(2)	102.00(7)	Group 2	BS
B010806p1	20.04(8)	7.00(9)	5.50(5)	25.80(9)	0.04(1)	0.180(4)	0.016(4)	43.2(1)	101.8(3)	Group 1	BS
B010806p2	23.73(4)	8.28(4)	6.47(7)	17.26(3)	0.03(1)	bdl	0.132(8)	45.64(7)	101.7(1)	Group 1	BS
∗B010806p3	23.8(1)	8.2(2)	6.32(8)	17.27(4)	0.02(3)	bdl	0.11(2)	45.5(2)	101.3(4)	Group 1	BS
B010806p4	23.6(1)	7.9(2)	6.4(2)	17.37(9)	0.018(7)	bdl	0.091(4)	45.2(2)	100.7(4)	Group 1	BS
∗B010806p5	20.1(1)	7.02(1)	5.47(7)	25.53(9)	0.032(9)	0.021(9)	0.10(4)	43.1(2)	101.5(4)	Group 1	BS,V
B010806p6	20.0(2)	7.05(5)	5.47(8)	25.41(2)	0.03(2)	0.171(1)	0.029(2)	43.0(2)	101.2(4)	Group 1	BS
B030806p1	23.7(2)	8.31(8)	6.42(3)	17.22(5)	0.05(1)	bdl	0.455(4)	45.6(2)	101.8(4)	Group 2	BS
∗B030806p2	20.2(1)	7.04(1)	5.4(1)	25.71(5)	0.05(2)	0.021(8)	0.38(4)	43.2(3)	101.9(6)	Group 2	BS
B030806p3	21.09(6)	7.30(4)	5.65(3)	24.10(2)	bdl	bdl	0.037(2)	43.88(7)	102.1(1)	Group 2	BS,V
B030806p4	23.2(4)	8.19(6)	6.51(2)	17.26(3)	0.02(1)	bdl	0.443(5)	45.1(4)	100.8(8)	Group 2	BS
B030806p5	20.0(1)	6.98(9)	5.4(2)	25.3(2)	0.02(2)	0.016(2)	0.354(5)	42.7(4)	100.7(9)	Group 2	BS,V

Figure in brackets is 1 standard deviation on the final digit

BS: Black specks; V: Vesicles

Table 3c: Results for Ni-bearing runs, continued

Sample	Si(wt%)	Al(wt%)	Mg(wt%)	Ca(wt%)	Fe(wt%)	S(wt%)	Ni(wt%)	O(wt%)	Total (wt%)	Group	Appearance
B140906p1	20.1(2)	6.9(1)	5.39(4)	25.46(4)	0.13(1)	0.206(1)	0.0258‡	43.1(2)	101.3(4)	Group 1	BS
B140906p2	20.1(2)	6.98(4)	5.21(5)	25.51(4)	0.06(1)	0.199(3)	0.0128‡	43.0(2)	101.1(4)	Group 1	BS
B140906p3	21.9(2)	7.2(3)	4.8(2)	23.5(1)	0.03(1)	0.1(1)	0.0066‡	44.05(3)	101.7(1)	Group 1	V
B140906p4	20.2(1)	6.96(7)	5.3(1)	25.68(6)	0.08(1)	0.203(3)	0.0299‡	43.2(2)	101.6(5)	Group 1	
B140906p5	20.18(9)	7.00(2)	5.28(6)	25.641(8)	0.104(7)	0.199(3)	0.0105‡	43.16(8)	101.6(1)	Group 1	
B140906p6	20.2(2)	6.98(6)	5.26(4)	25.62(4)	0.08(1)	0.207(3)	0.0267‡	43.1(2)	101.5(3)	Group 1	
B190906p1	20.2(2)	7.09(7)	5.5(2)	24.6(2)	bdl	bdl	0.005(3)	42.8(4)	100.2(1)	Group 4	BS,V
B190906p2	19.39(1)	6.79(8)	5.3(1)	23.09(2)	0.034(7)	bdl	4.25(2)	41.9(2)	100.7(4)	Group 4	BS
B190906p3	18.7(1)	6.47(7)	5.00(9)	23.61(9)	0.03(1)	bdl	5.64(4)	41.1(1)	100.5(3)	Group 4	BS,V
B190906p4	18.5(1)	6.3(2)	4.57(2)	23.6(2)	0.050(4)	bdl	6.38(7)	40.68(7)	100.1(2)	Group 4	BS
B190906p5	19.8(1)	6.84(8)	5.40(4)	24.1(1)	0.020(5)	bdl	2.473(7)	42.4(2)	101.0(4)	Group 4	
B190906p6	19.13(4)	6.52(6)	4.99(8)	22.15(4)	0.04(2)	bdl	6.45(5)	41.28(9)	100.6(2)	Group 4	
B191006p1	20.1(1)	7.02(6)	5.32(8)	25.42(8)	0.05(1)	bdl	0.084(5)	42.8(1)	100.9(3)	Group 3	BS
B191006p2	19.7(3)	6.9(2)	5.3(1)	25.2(5)	0.03(1)	bdl	0.349(1)	42.3(7)	100.(2)	Group 3	BS
B191006p3	20.0(1)	6.97(1)	5.39(1)	25.58(7)	0.04(1)	bdl	0.292(7)	42.9(2)	101.2(3)	Group 3	
B191006p4	19.57(9)	6.79(3)	5.37(1)	25.25(7)	0.03(2)	bdl	0.429(5)	42.1(2)	99.7(4)	Group 3	BS, V
B191006p5	19.8(2)	6.82(5)	5.36(6)	25.21(6)	0.066(8)	bdl	0.65(2)	42.5(2)	100.7(4)	Group 3	BS, V
B191006p6	20.0(2)	6.88(1)	5.39(5)	25.43(7)	0.050(7)	bdl	0.87(3)	42.9(2)	101.6(4)	Group 3	BS

Figure in brackets is 1 standard deviation on the final digit

‡:Laser analysis

BS: Black specks; V: Vesicles

Table 3d: Results for Cu-bearing runs

Sample	Si(wt%)	Al(wt%)	Mg(wt%)	Ca(wt%)	Fe(wt%)	S(wt%)	Cu(wt%)	O(wt%)	Total(wt%)	Appearance
B040106p1	20.1(1)	6.73(7)	5.11(3)	25.15(6)	0.042(2)	0.035(2)	0.00066‡	42.29(9)	99.4(2)	
B040106p2	20.0(1)	6.60(9)	5.11(2)	24.98(4)	0.051(9)	0.0338(5)	0.00072‡	42.0(2)	98.8(4)	
B040106p3	20.2(1)	6.76(4)	5.032(5)	24.98(3)	0.042(2)	0.0330(4)	0.00071‡	42.4(2)	99.4(3)	
B040106p4	20.16(9)	6.75(2)	5.22(4)	25.01(5)	0.043(4)	0.0346(8)	0.00076‡	42.45(9)	99.7(2)	BS
B040106p5	20.2(2)	6.70(6)	5.17(5)	24.96(4)	0.045(7)	0.035(1)	0.00072‡	42.4(3)	99.5(6)	
B040106p6	19.97(9)	6.73(5)	5.19(3)	25.09(3)	0.041(7)	0.0348(1)	0.00073‡	42.2(1)	99.3(3)	
B210306p1	20.1(1)	7.36(3)	5.55(4)	25.24(4)	0.03(2)	0.027(2)	0.039(3)	43.2(2)	101.5(3)	BS
B210306p2	19.9(2)	7.30(7)	5.55(9)	25.31(6)	0.04(1)	0.027(3)	0.043(2)	43.0(2)	101.2(4)	BS
B210306p3	19.8(2)	7.3(1)	5.52(9)	25.24(9)	0.05(1)	0.026(5)	0.037(2)	42.8(3)	100.7(7)	BS
B210306p4	18.6(4)	6.83(7)	5.20(8)	24.5(4)	0.03(1)	0.028(6)	0.040(5)	40.5(7)	96.(2)	BS
B210306p5	18.60(9)	6.9(1)	5.31(7)	24.8(1)	0.05(1)	0.026(6)	0.051(8)	40.8(2)	96.5(4)	BS
B210306p6	19.4(3)	7.2(1)	5.41(6)	24.6(2)	0.06(1)	0.028(3)	0.055(9)	41.9(6)	99.(1)	

Figure in brackets is 1 standard deviation on the final digit

‡:Laser analysis

BS: Black specks; V: Vesicles

Table 4: Coefficients for Eqn 3

Parameter	value	s.d.
A_0	-14.286	0.05
A_{Ca}	7.56	0.13
A_{Mg}	4.48	0.13
A_{NaorK}	4.24	0.79
A_{Fe}	26.31	0.24
A_{Al}	1.06	0.18
A_{Mn}	29.5	1.7
A_{W}	8.5	6.9

Table 5: Model performance summary

Model	mean(residuals)	σ(residuals)	R^2	NMRSD
WC1992	0.014	0.162	0.894	0.147
SC2005	-0.085	0.144	0.882	0.151
OM2002	-0.014	0.181	0.913	0.164
MO2005	0.043	0.098	0.965	0.096

WC1992: Wallace and Carmichael 1992

SC2005: Scaillet and Pichavant 2005

OM2002: O'Neill and Mavrogenes 2002

OM2005: Moretti and Ottonello 2005

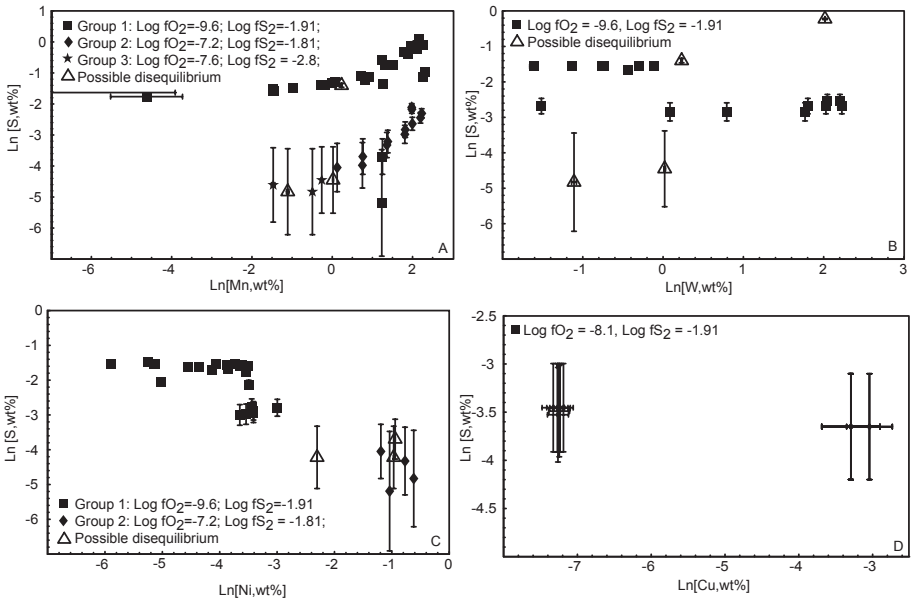
Group 1: Log fO2=-9.6; Log fS2=-1.91;
Group 2: Log fO2=-7.2; Log fS2=-1.81;
Group 3: Log fO2=-7.6; Log fS2 = -2.8;
Possible disequilibrium
Ln [S,wt%]
Ln[Mn,wt%]
A
Log fO2 = -9.6, Log fS2 = -1.91
Possible disequilibrium
Ln [S,wt%]
Ln[W,wt%]
B
Group 1: Log fO2=-9.6; Log fS2=-1.91
Group 2: Log fO2=-7.2; Log fS2 = -1.81;
Possible disequilibrium
Ln [S,wt%]
Ln[Ni,wt%]
C
Log fO2 = -8.1, Log fS2 = -1.91
Ln [S,wt%]
Ln[Cu,wt%]
D

Fig. 1.

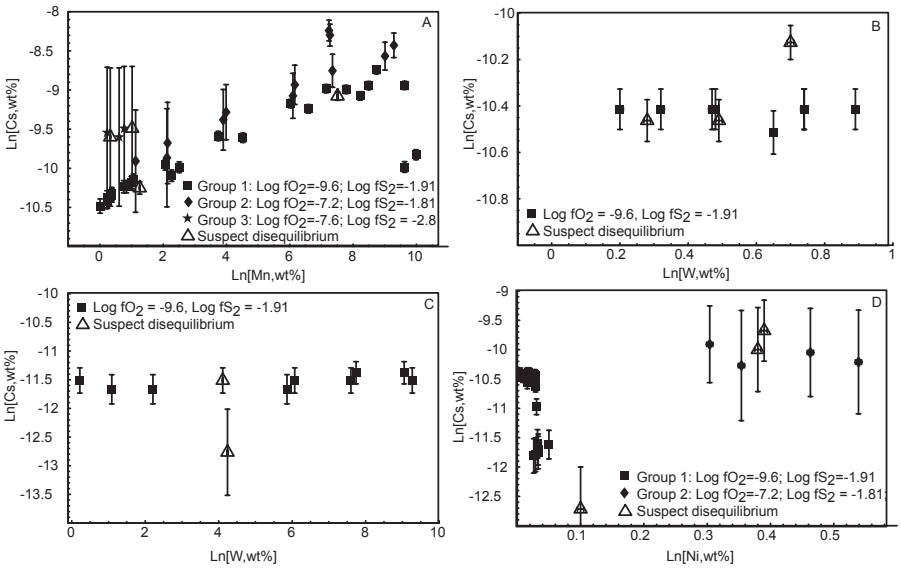
A
Ln[Cs,wt%]
Ln[Mn,wt%]
Group 1: Log fO2=-9.6; Log fS2=-1.91
Group 2: Log fO2=-7.2; Log fS2=-1.81
Group 3: Log fO2=-7.6; Log fS2 = -2.8
Suspect disequilibrium
B
Ln[W,wt%]
Log fO2 = -9.6, Log fS2 = -1.91
Suspect disequilibrium
C
Ln[W,wt%]
D
Ln[Ni,wt%]
Group 1: Log fO2=-9.6; Log fS2=-1.91
Group 2: Log fO2=-7.2; Log fS2 = -1.81

Fig. 2.

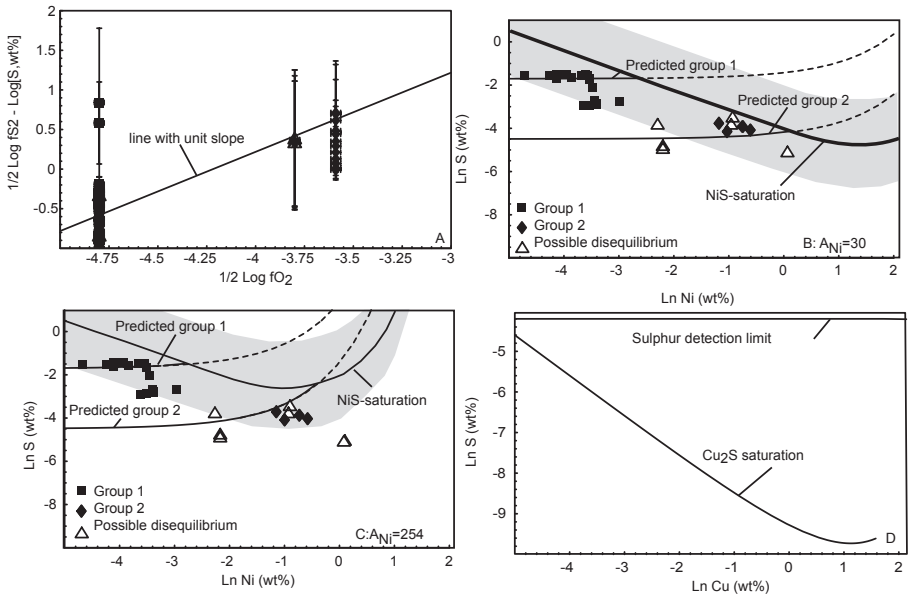
1/2 Log fS2 - Log[S, wt%]
1/2 Log fO2
line with unit slope
A
Ln S (wt%)
Ln Ni (wt%)
Predicted group 1
Predicted group 2
NiS-saturation
Group 1
Group 2
Possible disequilibrium
B: A_Ni=30
C:A_Ni=254
Sulphur detection limit
Cu2S saturation
D
Ln Cu (wt%)

Fig. 3.

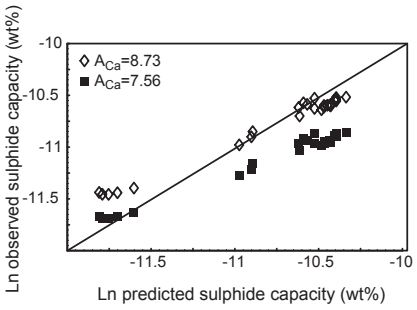
Ln observed sulphide capacity (wt%)
-10
-10.5
-11
-11.5
◇ A_{Ca}=8.73
■ A_{Ca}=7.56
-11.5
-11
-10.5
-10
Ln predicted sulphide capacity (wt%)

Fig. 4.

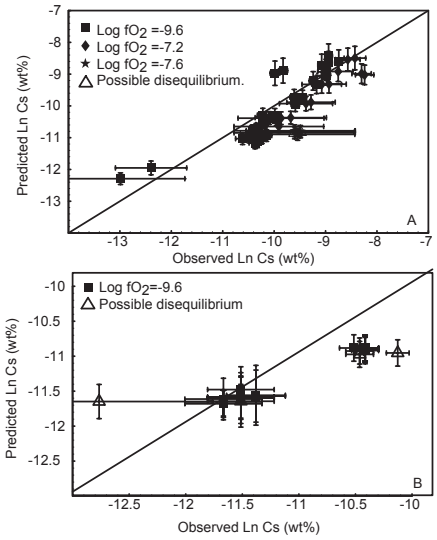
Log fO2 =-9.6
Log fO2 =-7.2
Log fO2 =-7.6
Possible disequilibrium.
Predicted Ln Cs (wt%)
Observed Ln Cs (wt%)
A
Log fO2=-9.6
Possible disequilibrium
Predicted Ln Cs (wt%)
Observed Ln Cs (wt%)
B

Fig. 5.

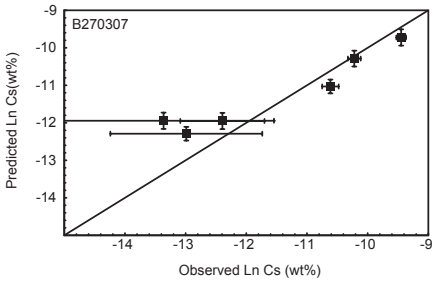

Fig. 6.

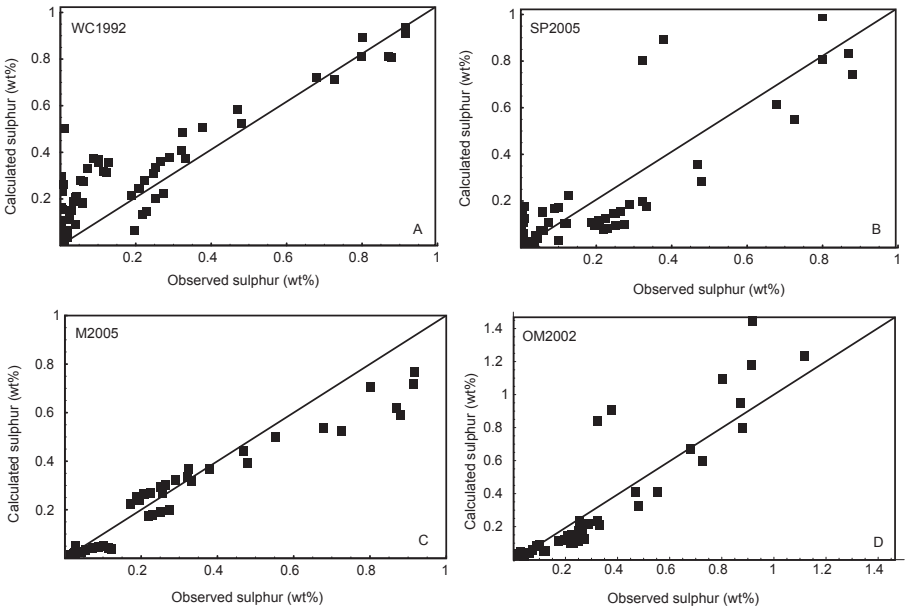
WC1992
A
SP2005
B
M2005
C
OM2002
D
Calculated sulphur (wt%)
Observed sulphur (wt%)

Fig. 7.